TIMP-3 in Bruch's Membrane: Changes during Aging and in Age-Related Macular Degeneration

主論文

Motohiro Kamei and Joe G. Hollyfield

Purpose. To assess the distribution, content, and function of tissue inhibitor of metalloproteinases (TIMP)-3 during aging in normal eyes for comparison with the levels observed in eyes with age-related macular degeneration (AMD).

Methods. Donor tissues analyzed included 36 normal eyes (14-96 years old) and 15 AMD eyes (74-98 years old). A tissue strip including the fovea was used for immunohistochemistry. Western blot analysis was performed on extracts of the retinal pigment epithelium (RPE)-choroid complex from the posterior part of each eye. Immunoreactivity of TIMP-3 bands in each western blot was densitometrically quantitated. The inhibitory function of TIMP-3 was evaluated with reverse zymography.

Results. TIMP-3 was present uniformly across Bruch's membrane in the normal samples. In samples from donors more than 50 years of age, immunostaining was intense. TIMP-3 content ranged from 92 to 1061 ng/cm^2 and increased with age ($r = 0.66$). In AMD eyes, TIMP-3 distribution in Bruch's membrane was abundant in areas of continuous soft drusen but absent in areas below RPE atrophy. TIMP-3 levels in AMD eyes were significantly higher than in age-matched normal eyes (577 versus 877 ng/cm^2; $P = 0.009$). Inhibitory activity correlated well with TIMP-3 content ($r = 0.82$) and was also significantly higher in AMD eyes than in age-matched normal eyes ($P < 0.001$).

Conclusions. During normal aging, TIMP-3 content in Bruch's membrane of the macula shows a significant increase. TIMP-3 content in AMD eyes was elevated relative to that of age-matched normal eyes. Higher levels of TIMP-3 may contribute to the thickening of Bruch's membrane observed in AMD. (*Invest Ophthalmol Vis Sci.* 1999;40:2367-2375)

Matrix metalloproteinases (MMPs) and the tissue inhibitors of matrix metalloproteinases (TIMPs) play important roles in regulating the turnover of the extracellular matrix (ECM). MMPs constitute a family of secreted enzymes, currently with more than 20 members, that are involved in degrading components of the ECM in the normal course of matrix turnover and renewal.[1] MMPs are also implicated during the initial stages of neovascularization, in which they are thought to be required, along with other proteases, for degradation of components of the capillary basement membrane as a prerequisite for new vessel outgrowth.[2] The TIMPs, which are represented by four distinct gene products, are thought to suppress excessive degradation of ECM and may play an important functional role in limiting neovascularization.[3-10]

TIMP-3 is unique in that once secreted, it binds to component(s) of the ECM, whereas other TIMPs do not.[11] In the outer eye wall, immunohistochemical studies indicate that TIMP-3 is present in normal Bruch's membrane,[12,13] and in situ hybridization studies indicate that the RPE is a major site of TIMP-3 gene expression.[14,15] One role of TIMP-3 in Bruch's membrane may be as a potent local inhibitor of MMP activity, regulating the rate of Bruch's membrane turnover, as well as limiting choroidal neovascularization.

Sorsby's fundus dystrophy is an early-onset, inherited form of macular degeneration, characterized by thickening of Bruch's membrane and submacular neovascularization, which are also features of AMD. Mutations in the gene coding for TIMP-3 have been found in families with Sorsby's fundus dystrophy.[16] Immunohistochemical studies of a donor eye from a Sorsby's patient showed extensive TIMP-3 accumulation in the thickened Bruch's membrane.[17] These observations led us to evaluate TIMP-3 content and distribution in Bruch's membrane of AMD donor eyes, which are known to accumulate drusen and exhibit abnormal thickening of this layer. Although no mutations in the coding region or the regulatory elements of the TIMP-3 gene have been discovered in patients with AMD to date,[18,19] excess TIMP-3 within the ECM could prevent normal matrix remodeling and could be causally involved in the increased thickening of Bruch's membrane that occurs in AMD.

Because of the importance of Bruch's membrane permeability in the trafficking of metabolites between choroid and RPE[20] and the known early alterations in this lamina in AMD,[21] it is important to understand the relationship of TIMP-3 in normal aging and AMD. In this study we follow the age-related changes in TIMP-3 distribution, content, and inhibitory activity during normal aging and compare these levels with those present in age-matched AMD donor eyes.

From The Eye Institute, The Cleveland Clinic Foundation, Ohio.

Supported by The Foundation Fighting Blindness and the Retina Research Foundation.

Submitted for publication January 20, 1999; revised April 9, 1999; accepted April 20, 1999.

Proprietary interest category: N.

Corresponding author: Motohiro Kamei, The Eye Institute, The Cleveland Clinic Foundation, 9500 Euclid Avenue FFB-33, Cleveland, OH 44195.

E-mail: kameim@cesmtp.ccf.org

TABLE 1. Normal Donor Eyes Used for TIMP-3 Analysis

No.	Age	Sex	Postmortem Time* (h)	Cause of Death	Weight† (mg)	Protein Concentration (mg/ml)	TIMP-3 Content (ng/cm²)	Relative Inhibitory Activity§
NOR-1	14	F	4/6	Auto accident	139	1.31	91.5	0.10
NOR-2	14	F	2/4	Asthma	138	1.55	161.6	0.15
NOR-3	16	F	1.5/4.5	Auto accident	198	1.90	177.7	0.27
NOR-4	18	F	2/2.5	Auto accident	156	1.94	215.4	0.21
NOR-5	29	M	6/5	Adenocarcinoma	178	1.58	113.1	0.21
NOR-6	39	M	2/10	Acute cardiac events	273	2.48	280.0	0.27
NOR-7	60	M	4/1	Acute cardiac events	176	1.35	295.1	0.64
NOR-8	61	M	2/NA	Acute myocardial infarction	169	1.73	317.7	0.58
NOR-9	61	M	4/1	Rupture of aortic aneurysm	202	2.07	210.0	0.47
NOR-10	62	F	4/2	Cardiomyopathy	155	1.39	430.8	0.65
NOR-11	63	F	4/4	Rupture of aortic aneurysm	202	2.00	486.3	0.83
NOR-12	65	M	4.5/4.5	Acute cardiac events	279	2.53	323.3	0.58
NOR-13	66	M	4/2	Acute cardiac events	175	1.20	590.7	0.90
NOR-14	69	F	3.5/10	Adenocarcinoma	224	1.78	405.0	0.59
NOR-15	70	F	4/5	Acute cardiac events	182	1.18	388.8	0.71
NOR-16	71	M	4/1	Acute cardiac events	122	1.28	507.3	0.51
NOR-17	71	F	5.5/13	Acute cardiac events	193	1.49	390.4	0.72
NOR-18	73	F	3/8	Acute cardiac events	289	1.37	329.0	0.54
NOR-19	81	M	2.5/4.5	Acute myocardial infarction	211	1.70	743.1	0.59
NOR-20	81	F	6.5/14	Pneumonia	205	1.56	700.1	0.77
NOR-21	83	F	3/4.5	Pneumonia	193	1.28	942.4	0.82
NOR-22	83	M	2.5/6.5	Congestive heart failure	164	1.73	463.1	0.58
NOR-23	85	F	6.5/5	Gastrointestinal bleeding	181	2.03	554.7	0.69
NOR-24	85	M	5.5/5	Sepsis	156	1.22	533.1	0.58
NOR-25	89	F	2.5/14	Pneumonia	226	1.13	576.2	0.55
NOR-26	90	F	5/6.5	Acute myocardial infarction	176	1.64	1060.8	0.83
NOR-27	92	M	2/NA	Acute myocardial infarction	130	1.18	263.9	0.66
NOR-28	93	F	5/11	Acute myocardial infarction	142	1.57	1010.0	0.63
NOR-29	93	F	7/6	Congestive heart failure	134	1.31	263.0	0.35
NOR-30	94	M	5/9	Squamous cell carcinoma	148	1.46	424.0	0.39
NOR-31	94	F	6/1	Respiratory failure	152	1.42	524.0	0.41
NOR-32	96	F	3/NA	Sepsis	147	1.07	710.8	0.90

NA, data not available.
* Postmortem time represented as death-enucleation/enucleation-freezing intervals.
† Weight refers to the isolated 10 × 10-mm sample used for TIMP-3 analysis.
§ Ratio (sample pixel density)/(standard pixel density).

METHODS

Donor Tissues

Thirty-two eyes from normal human donors (Table 1) and 15 eyes from AMD donors (Table 2) were used. Normal eyes were obtained through the Cleveland Eye Bank , Ohio, and the National Disease Research Interchange (Philadelphia, PA). They were enucleated between 1.5 and 7 hours after death and preserved at 4°C for 1 to 14 hours. Immediately after arrival at our laboratory or National Disease Research Interchange, they were frozen in liquid nitrogen and stored at −80°C until sample preparation. AMD donor eyes were obtained through the Eye Donor Program of the Foundation Fighting Blindness (Hunt Valley, MD). They were enucleated between 1.5 and 8 hours after death and retained at 4°C for 0.5 to 11.5 hours before freezing in liquid nitrogen before storage at −80°C.

Tissue Preparation

Each tissue sample consisted of a 10 × 12 mm rectangle, cut from the posterior pole of the frozen globe, temporal to the optic nerve head. The exact area to be removed was first defined with vernier calipers using the optic nerve, the long posterior ciliary artery and the insertion of the inferior oblique muscle as external markers to localize the position of the fovea internally. An incision through the sclera into the vitreous was made on each side of the rectangle to free the sample. A 2-mm-wide strip of the retina-RPE-choroid-sclera complex, centered on the fovea, was separated for immunohistochemistry.

For biochemical samples, the retina, any adhering vitreous, and sclera were removed from the remaining 10 × 10-mm aerial expanse of tissue and the RPE-Bruch's membrane-choroid complex was retained for extraction. Each sample was weighed and then homogenized in 350 μl of extraction buffer, consisting of 500 mM Tris-HCl (pH 7.6), 200 mM NaCl, 1% Triton X-100, and protease inhibitors (400 μg/ml EDTA, 0.5 μg/ml leupeptin, 0.7 μg/ml pepstatin, and 100 μg/ml phenylmethylsulfonyl fluoride). After incubation for 15 minutes on ice followed by centrifugation at 13,000 rpm for 30 minutes at 4°C, the supernatant was collected and stored at −70°C. Protein concentration of each sample was measured using bicin-

TABLE 2. AMD Donor Eyes Used for TIMP-3 Analysis

No. (FFB accession no.)	Age	Sex	Postmortem Time* (h)	Cause of Death	Weight† (mg)	Protein Concentration (mg/ml)	TIMP-3 Content (ng/cm²)	Relative Inhibitory Activity§	Hard Drusen	Soft Drusen	CNV (mm)	Atrophy (mm)
AMD-1 (359)	74	F	2.5/2	Ruptured aortic aneurysm	127	1.16	755.5	1.13	−	++	0	2
AMD-2 (511)	76	F	8/2	Acute myocardial infarction	265	1.56	960.1	1.37	+	+	0	4
AMD-3 (503)	77	F	4/1	Acute myocardial infarction	197	1.73	378.6	0.94	+	+	5.5	6
AMD-4 (321)	78	F	1.5/1.5	Lung carcinoma	192	1.45	348.4	0.61	+	+	0	0.5
AMD-5 (429)	78	M	11‡	Acute myocardial infarction	165	1.34	739.4	1.11	++	+	0	5.5
AMD-6 (446)	84	F	7.5/3.5	Liver failure	187	1.75	1207.9	1.22	++	++	2	2.5
AMD-7 (444)	84	F	6/1.5	Pneumonia	198	1.58	1015.1	0.95	+	++	4.5	7.5
AMD-8 (334)	86	F	6/NA	Cancer	182	1.38	1060.8	0.94	+	+	6	6
AMD-9 (344)	88	F	3/1	Respiratory failure	214	2.53	488.4	0.99	−	+	6.5	8.5
AMD-10 (532)	91	F	5/4	Acute respiratory arrest	176	1.60	877.8	0.95	−	+	5	6
AMD-11 (447)	92	M	3/11.5	Ischemic cardiomyopathy	224	1.61	1062.5	1.42	+	++	0	6.5
AMD-12 (433)	93	M	7.5/NA	Sepsis	208	1.39	628.4	0.88	+	+	0	0
AMD-13 (450)	94	F	7/3	Acute myocardial infarction	169	1.38	1498.6	1.69	++	++	2	2.5
AMD-14 (353)	95	F	3/0.5	Acute myocardial infarction	102	1.30	928.9	1.00	++	++	0	0
AMD-15 (EB)	98	F	4/1	Congestive heart failure	198	1.78	1202.5	1.12	+	++	3	3.5

CNV, choroidal neovascularization; NA, data not available; EB, donation obtained directly from a local eyebank.
* Postmortem time represented as death-enucleation/enucleation-freezing intervals.
† Weight refers to the isolated 10 × 10-mm sample used for TIMP-3 analysis.
‡ Total interval from death to freezing.
§ Ratio (sample pixel density)/(standard pixel density).

choninic acid (BCA; Pierce, Rockford, IL) and bovine serum albumin (BSA) as a reference standard.

TIMP-3 content was evaluated as the amount per area (10 × 10 mm²). Wet tissue weight and protein content of each sample are presented in Tables 1 and 2.

Immunohistochemistry

The 2 × 10-mm tissue strip including the fovea was embedded in optimum cutting temperature (OCT) compound (Tissue-Tek, Sakura Finetek, Torrance, CA) and frozen in liquid nitrogen for immunocytochemistry in the absence of fixation. Indirect immunohistochemistry was performed on 8-μm-thick cryosections. After quenching endogenous peroxidase activity with 0.3% hydrogen peroxide and blocking nonspecific antibody binding with 5% BSA in PBS containing 0.3% Triton X-100, the sections were incubated overnight at 4°C with a mouse monoclonal anti-human TIMP-3 antibody (either Clone 136-13H4, provided by Suneel Apte or 136-17B12, provided by Kazushi Iwata, [Fuji Chemical Industries, Toyama, Japan]). The primary antibody was used at 1:1000 dilution. Biotinylated horse anti-mouse IgG (1:200 dilution; Vector, Burlingame, CA) was used as a secondary antibody followed by the avidin-biotin complex method (Elite ABC, Vector). Immunoreactivity was resolved with horseradish peroxidase-aminoethylcarbazole, which produces a magenta reaction product. Sections were counterstained with hematoxylin. Control sections were prepared in an identical manner with the exception that non-immune mouse IgG was used as the primary antibody.

Microscopic Evaluation

Because no detailed clinical history was available on any of the donor eyes classified as AMD, it was necessary to evaluate the status of the disease in the AMD donor tissues based on the histopathology of the tissue samples. For classification of the AMD disease status, we assessed the following criteria, also used in the recently published ARMD Grading System[22]: hard drusen status: (−) no hard drusen, (+) 1 to 3 hard drusen in the 10-mm section, (++) 4 or more hard drusen in the 10-mm section; soft drusen status: (−) no soft drusen, (+) patchy soft drusen present but not continuous, (++) continuous soft drusen extending more than 0.5 mm; the presence and length of choroidal neovascular membranes; and RPE atrophy measured in the full 10-mm length of the section. We could not evaluate basal laminar or linear deposits, because these features cannot be distinguished within drusen with light microscopy on unfixed tissue samples. The listed features are presented for each AMD donor eye in Table 2.

Western Blot Analysis

Immediately before electrophoresis, 3.5 μl of sample buffer (4× NuPage sample buffer, Novex, San Diego, CA) containing dithiothreitol (final concentration, 50 mM) was added to 6.5 μl of the protein extract. The 4× sample buffer (pH 8.5) consisted of 1.17 M sucrose, 563 mM Tris base, 423 mM Tris-HCl, 278 mM sodium dodecyl sulfate (SDS), 2.05 mM EDTA, 0.88 mM Coomassie Blue R250 and 0.70 mM phenol red. After heating for 10 minutes at 70°C, 10-μl volumes of each sample were loaded into gel slots for electrophoresis on 10% gels (Bis-Tris; Novex) with 2-(*N*-morpholino) ethane sulfonic acid SDS running buffer (NuPage MES-SDS; Novex). Recombinant human TIMP-3 protein (10 ng) was included in a separate lane as a positive control. Proteins were transferred from the gel to polyvinylidene difluoride membranes using blotting apparatus (XCell II; Novex). After transfer, membranes were incubated with blocking solution (2% BSA in Tris-buffered saline) for 1 hour. The monoclonal anti-human TIMP-3 antibody (Clone 136-17B12) conjugated to horseradish peroxidase was applied at 1:1000 dilution and incubated overnight at 4°C. After rinsing, immunoreactivity was displayed with the chemiluminescent method (ECL, Amersham, Arlington Heights, IL) and captured on radiographic film during a 10- to 15-second exposure. The immunoreactivity signal was digitized on a Scanwizard (Microtek, Redondo Beach, CA) flatbed scanner. The intensity of immunoreactivity was quantitated from the digitized images using commercial software (Digital Science 1D; Eastman Kodak, Rochester, NY) on a personal computer (Power Macintosh, Apple Computer, Cupertino, CA). The densitometric intensity was converted to amount of protein (nanograms per sample) by comparing the intensity of immunoreactivity with that of varying amounts of recombinant TIMP-3 standard.

Protein Isolation and N-Terminal Sequence Analysis

In addition to recognizing the TIMP-3 bands at 24 and 27 kDa, the monoclonal antibody also interacted with two additional bands at 37 and 40 kDa. To determine whether these were aggregates of TIMP-3 or unrelated proteins, we excised the higher molecular weight bands from polyvinylidene difluoride membrane after electrotransfer from a separate gel and analyzed the bands by Edman microsequencing using a (Procise 492; PE Biosystems, Foster City, CA) protein sequencer in the Molecular Biology Core Laboratory, Case Western Reserve University (Cleveland, OH).

Reverse Zymography

TIMP-3 functional activity in each sample was established with reverse zymography using protease-substrate gel electrophoresis, as described previously.[11] In brief, the extracted protein from the RPE-choroid complex was diluted to 75 times and activated by adding calcium chloride at a final concentration of 10 mM. After mixing with 4× loading buffer (40 mM Tris, 8% SDS, 40% glycerol, and 0.01% bromphenol blue), 20 μl of the sample (without heating or reducing agents) was separated by electrophoresis in a matrix consisting of 0.1% SDS, 12% polyacrylamide gel containing MMP-2, MMP-9, and 0.1% gelatin (from a reverse zymography kit which also includes TIMP-3 standards provided by Dylan R. Edwards, The University of Calgary, Alberta, Canada). To remove SDS, the gel was rinsed overnight in the following buffer (50 mM Tris [pH 7.5], 5 mM $CaCl_2$, and 25 mg/ml Triton X-100). The gel was then placed in an incubation buffer (50 mM Tris [pH 7.5] and 5 mM $CaCl_2$) to allow MMPs to degrade gelatin for 24 hours at 37°C. Coomassie blue stains only the protein (gelatin) in the region where MMP activity has been inhibited. Intensity of the Coomassie blue-stained gelatin was quantitated as described earlier. The values obtained were compared with the intensity of Coomassie blue staining of the gelatin in lanes with known concentrations of TIMP-3 standards.

Statistical Analysis

Western blot analysis and reverse zymography were repeated three times on each sample. The results are expressed as the mean ± 1 SD.

Diversity of tissue weight and protein concentration of samples were analyzed with unpaired Student's *t*-test. Correlations between TIMP-3 content and age or inhibitory activity were determined with Pearson's correlation coefficient. Differences in TIMP-3 content and inhibitory activity between AMD and age-matched normal tissue were analyzed with the Mann-Whitney test.

Results

TIMP-3 Distribution and Content in Normal Eyes

Table 1 presents a summary of all the data and vital information from each normal eye used in this analysis.

Distribution. TIMP-3 immunoreactivity was present in Bruch's membrane in each normal donor tissue used and was distributed across the full thickness of this membrane. Although immunoreactivity was uniform in each donor sample, in general, eyes from younger donors showed less intense immunostaining than eyes from older donors. In addition to TIMP-3 immunolocalization in Bruch's membrane, samples from 80- and 90-year-old donors commonly exhibited intense staining in the capillary bed matrix. TIMP-3 immunoreactivity was not evident in the neurosensory retina, the choroid, or the sclera. In the control tissues where nonimmune mouse IgG was substituted for the monoclonal IgG, Bruch's membrane showed no immunoreactivity. Examples of TIMP-3 immunolocalization from donors at a variety of representative ages are presented in Figure 1.

Content. Western blot analysis with the TIMP-3 antibody revealed a major 24-kDa band and a minor 27-kDa band in each of the RPE-choroid tissues samples (Fig. 2). The 27-kDa band was identical in location to the recombinant glycosylated form of TIMP-3, used as a positive control. The 24-kDa band is reported to correspond to the unglycosylated form of TIMP-3 .[5]

Two additional minor bands at 37 and 40 kDa were also detected by the antibody. These bands were separately isolated from electroblotted polyvinylidene difluoride membrane and analyzed by microsequencing. The 37-kDa band yielded an N-terminal sequence of GKVKVGVNGFSRIIQLVTRAA, which corresponds 100% to the N terminus of human glyceraldehyde-3-phosphate dehydrogenase (GAPDH, accession no. X01677). Authentic GAPDH (Boehringer Mannheim, Indianapolis, IN) was used in western blot analyses to evaluate cross-reactivity with the anti-TIMP-3 antibody. Cross-reactivity was evident when at least 125 ng GAPDH was loaded, but was not detected when lower loading levels were applied (data not shown).

The 40-kDa immunoreactive band yielded the N-terminal

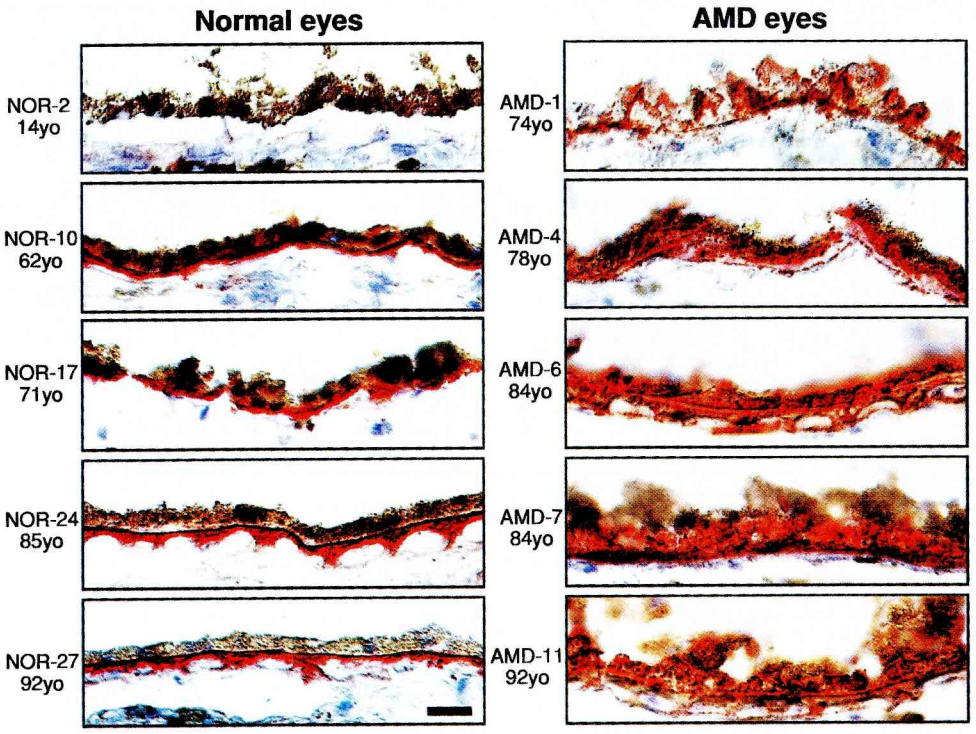

FIGURE 1. TIMP-3 immunolocalization in the normal and AMD donor eyes at the indicated ages. TIMP-3 immunoreactivity in Bruch's membrane is uniform in each normal sample. The younger donor eyes, especially those from the second or third decade, showed less intense immunostaining than the older donor eyes. In the samples from 80- and 90-year-old normal donors eyes, intense staining was also commonly observed extending into the capillary bed matrix. In AMD eyes, note the areas with continuous soft drusen, which show intense immunoreactivity with the TIMP-3 antibody. Original magnification, ×500; bar, 20 μm.

sequence of LAIPALAQEQPQGQ, which shows less than 40% homology to any known protein. Although the identity of this 40-kDa protein was not established, the sequence obtained did not identify this protein as an aggregate of TIMP-3.

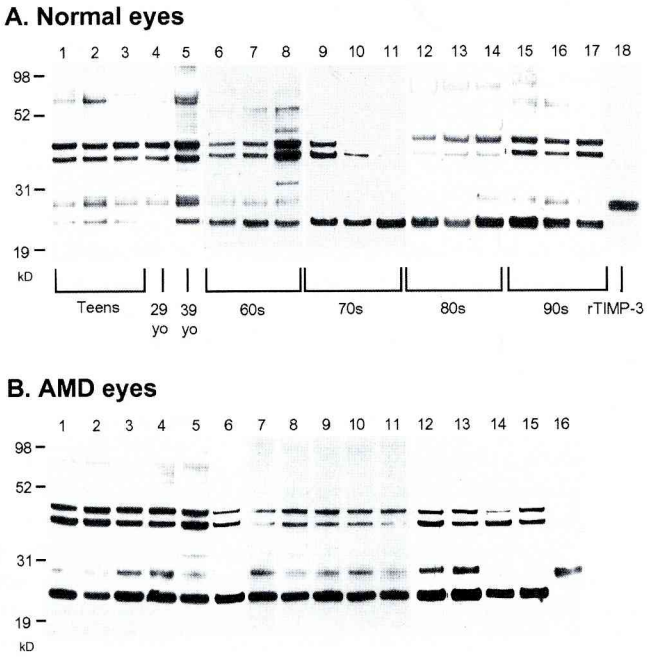

FIGURE 2. Western blot of the samples from normal (**A**) and AMD (**B**) donors. The 27-kDa band in *lanes 1* through *17* is identical in location with the recombinant glycosylated form of TIMP-3 used as a standard in *lane 18*. The 24-kDa band, which shows the most intense signal, particularly from the older donor eyes, corresponds to the unglycosylated form of TIMP-3. The intensity of the bands appears to increase with age in the samples from normal donors. All the samples from AMD donor eyes show intense immunoreactivity.

The immunoreactivity present in the 24- and 27-kDa western blot bands was variable among different samples. Notably, the relative amounts of immunoreactivity were found to be age dependent, with less intense signals present in samples from young donors than from older donors. Densitometric measurements of specific TIMP-3 immunoreactivity in the 24- and 27-kDa bands suggest that the TIMP-3 content ranged from a low of 92 ng/cm^2 in a sample from a 14-year-old donor of normal eyes to 1061 ng/cm^2 in a sample from a 90-year-old donor of normal eyes (Table 1). A direct relationship between TIMP-3 content and age (Fig. 3) appears to be significant in all the normal tissue analyzed (correlation coefficient, $r = 0.66$; $n = 32$).

To evaluate the influence of postmortem intervals on protein degradation, we performed semiquantitative western

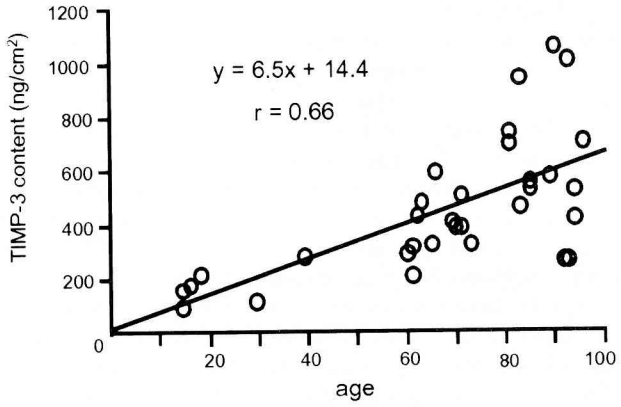

FIGURE 3. The relationship between TIMP-3 content and age of normal donor eyes. Densitometric measurements of the specific TIMP-3 immunoreactivity in the 24- and 27-kDa bands, when converted to protein amounts, show an age-dependent increase in concentration with a significant correlation coefficient ($r = 0.66$).

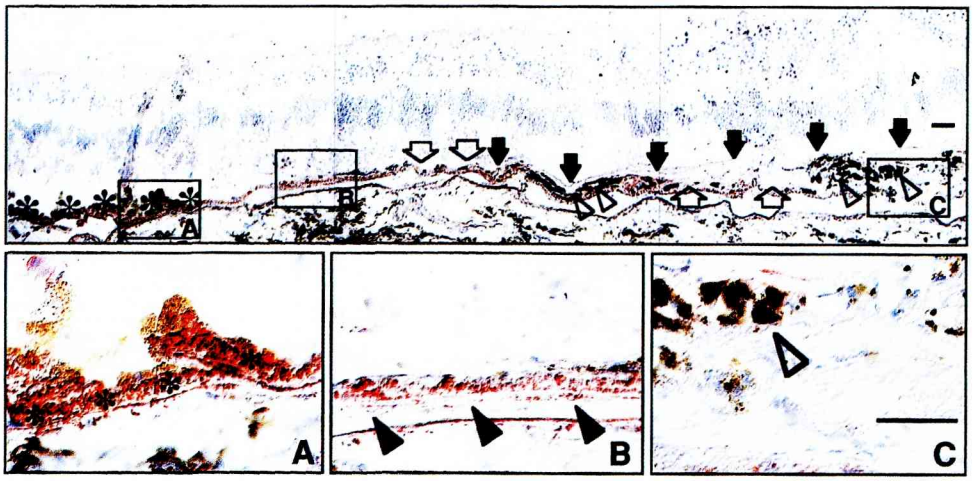

FIGURE 4. Frozen section of an AMD eye (AMD-15) showing representative features including continuous soft drusen (*asterisks*), an area with RPE atrophy (*open arrows*), and choroidal neovascularization (*arrows*). A region of transition is seen with apparently normal RPE on the *left* side of the image that continues into an area with RPE atrophy on the *right* side of the figure. Three areas from the lower magnification image at the top are shown at higher magnification in the lower three panels. The area with continuous accumulation of soft drusen with an intact RPE shows intense TIMP-3 immunoreactivity (**A**). In regions of transition between areas of RPE atrophy and a normal RPE, TIMP-3 immunoreactivity decreases but is still present in soft drusen and below the central elastin layer of Bruch's membrane (*arrowheads*; **B**). TIMP-3 immunoreactivity is not present in the area of choroidal neovascularization with RPE atrophy but is present surrounding the hyperplastic RPE (*open arrowhead*; **C**). Original magnification, ×125 (*top*); ×500 (*bottom*); bars, 20 μm.

blot analysis after incubating tissue buttons punched out from one eye for various intervals at room temperature. The results showed no apparent change for 12 hours but a decrease after 24 hours (data not shown). This indicates that TIMP-3 can be a considerably stable molecule with six pairs of disulfide bonds. Therefore, it is reasonable to use samples with various postmortem intervals as long as the samples are stored less than 12 hours at room temperature. The donor eyes used in this study were enucleated within 8 hours and kept at 4°C until frozen, which was within 12 to 14 hours after enucleation.

TIMP-3 Distribution and Content in AMD Eyes

Table 2 presents the summary of all the data and vital information from each AMD eye used in this analysis.

Distribution. Representative examples of several features characteristic of AMD eyes are shown in Figure 4. Each AMD eye used contained soft drusen, with 7 of the 15 samples having a continuous expanse of soft drusen for the full 10-mm length of the sample section examined. Whenever soft drusen were observed, whether isolated or continuous, each was intensely immunoreactive with the TIMP-3 antibody (Figs. 1, 4A). Hard drusen, when present, were also strongly immunoreactive. Most of the AMD donor tissues (13 of 15) contained areas of RPE atrophy, which involved from 0.5 to 8.5 mm of the 10-mm section length examined. In Bruch's membrane below the expanses of RPE atrophy, TIMP-3 immunoreactivity was either not evident or barely detectable (Fig. 4C). Choroidal neovascularization was present in 8 of the 15 AMD donor eyes. RPE atrophy, where little or no TIMP-3 immunoreactivity was present, as described earlier, was always noted below the areas of choroidal neovascularization (Fig. 4). In areas where the RPE had proliferated around a choroidal neovascular membrane or a fibroblastic scar, TIMP-3 immunoreactivity was observed surrounding the hyperplastic RPE (Fig. 4C). The immunoreactivity is subtle, however, and shows irregular distribution, possibly because of a loss of function and polarity of the proliferated RPE. In regions of transition between areas of RPE atrophy and a normal RPE, TIMP-3 immunoreactivity decreases but is still present in soft drusen and below the central elastin layer of Bruch's membrane (Fig. 4B).

Content. In general, AMD samples showed more intense immunoreactivity in western blot analysis when compared with age-matched normal eyes. Average densitometric analysis suggests that TIMP-3 content in AMD eyes was 877 ± 325 ng/cm^2 (n = 15) and 577 ± 241 ng/cm^2 in the age-matched normal eyes (n = 18). The measurements demonstrating this apparent difference in TIMP-3 content in the macular region between AMD and normal eyes were statistically significant (P = 0.009; Fig. 5).

TIMP-3 Function in Normal and AMD Eyes

The inhibitory activity of TIMP-3 was evaluated with reverse zymography. In each sample analyzed, a densely staining gelatin band remained in the zymograms at 24 kDa and a minor stained band remained at 27 kDa, identical with the results of recombinant TIMP-3 (Fig. 6). Inhibitory activity was not present in areas of the zymograms above 27 kDa. Some samples also showed gelatin remaining at 21 and 22 kDa. The 21-kDa band was identical with the band of recombinant TIMP-2. No inhibitory activity was observed in the location corresponding to TIMP-1 (at 28.5 kDa). The identity of the inhibitor present at the 22-kDa location has not been established; this could represent a partially degraded form of TIMP-3 or an as yet undescribed member of the TIMP family. The intensity of staining of the remaining gelatin in the 24- and 27-kDa locations varied with samples from 0.10 to 1.69 arbi-

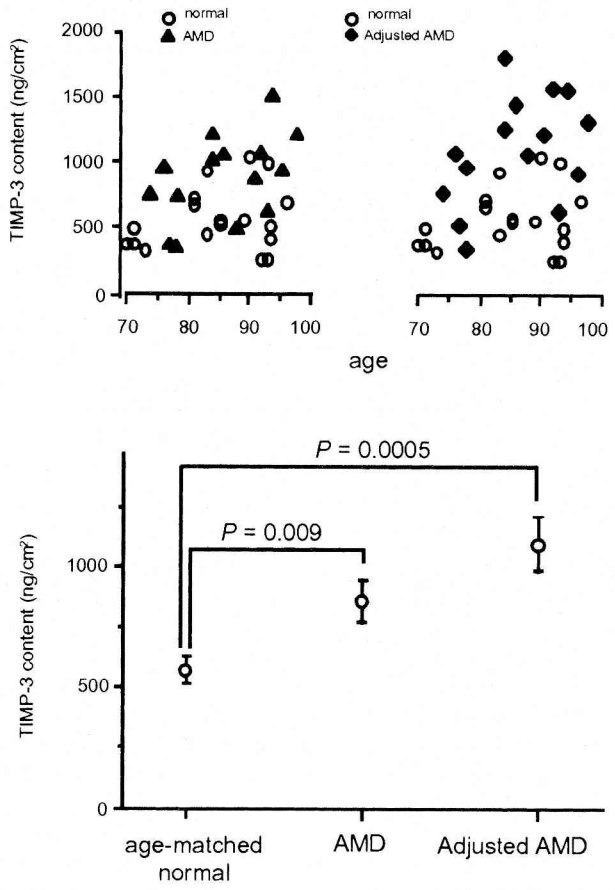

Figure 5. TIMP-3 content as a function of age in AMD samples and age-matched normal samples (*top left*) after adjustment in AMD (*top right*) and comparison between these groups. The difference in TIMP-3 content in the macula between AMD (877 ± 325 ng/cm^2) and normal eyes (577 ± 241 ng/cm^2) was statistically significant. The adjustment suggests that the TIMP-3 level below areas where the RPE remains (1106 ± 420 ng/cm^2) is approximately two times higher in AMD eyes than in age-matched normal eyes. ○, normal samples; ▲, AMD samples; ♦, adjusted AMD samples.

trary densitometric units. TIMP-3 function showed a significant correlation with age in the normal eyes ($r = 0.67$; $n = 32$) and was highly correlated with TIMP-3 content in all macular samples ($r = 0.82$, $n = 47$; Fig. 7). Notably, TIMP-3 inhibitory activity detected by reverse zymography was elevated approximately twofold in the AMD eyes compared with the age-matched normal eyes ($P < 0.001$; Fig. 8).

Discussion

The amount of functional TIMP-3 present in Bruch's membrane below the macula of the normal human retina appears to be age dependent. Sections from the fovea of the donors from the second and third decade of life were weakly immunoreactive with anti-TIMP-3 antibody. This correlated well with lower amounts of immunoreactivity observed in western blot analysis. Additionally, TIMP-3 distribution changed in the 9th and 10th decade samples, with extension of immunoreactivity from Bruch's membrane into the matrix surrounding the choriocapillaris. Quantitative analysis showed that TIMP-3 content and function in the macula increased with age with a significant correlation coefficient ($r = 0.66$ and 0.67, respectively). Proteins that increase or decrease with age can be referred to as senescence-related proteins and are candidate molecules for age-related diseases.[23,24] Accordingly, we propose that TIMP-3 is a senescence-related protein.

Immunostaining of TIMP-3 was conspicuous in extensive accumulation of drusen, which is characteristic of AMD eyes. Quantitative analysis showed that TIMP-3 levels were significantly elevated in the macula of AMD eyes compared with normal eyes. AMD eyes, however, showed a nonuniform distribution, with virtually no TIMP-3 immunoreactivity below the area of RPE atrophy and abundant immunoreactivity in the area outside the atrophic areas where the RPE was present, which is consistent with the observation in Sorsby's fundus dystrophy and retinitis pigmentosa.[17] This indicates that TIMP-3 distribution in AMD eyes with RPE atrophy is nonuniform. To determine the TIMP-3 content below areas where the RPE remains, we assumed that the area of RPE atrophy was circular and that

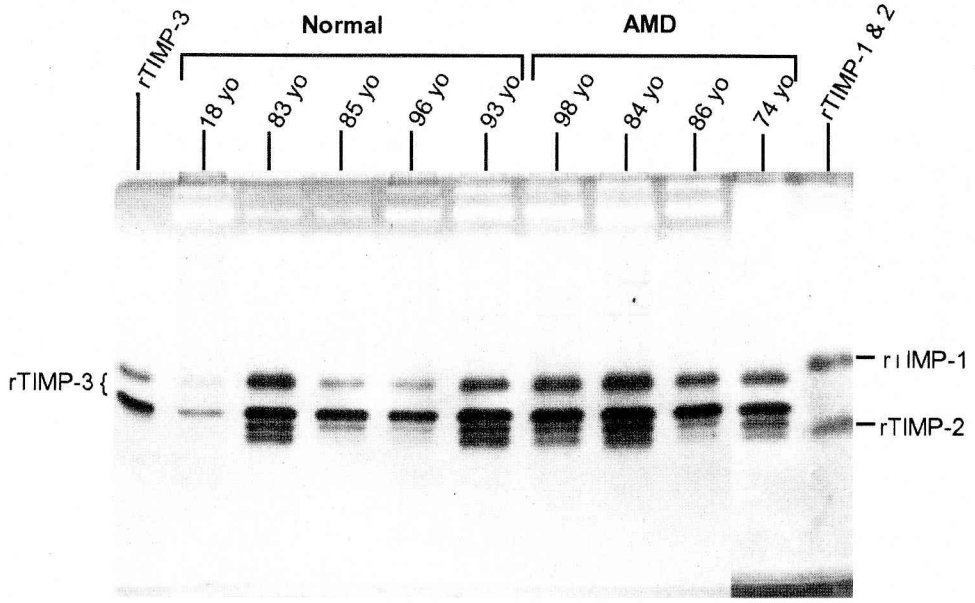

Figure 6. Reverse zymography of normal and AMD samples. Gelatin bands stained with Coomassie blue are seen at 24 and 27 kDa, whose locations are identical with those of the recombinant TIMP-3. Some samples also show gelatin remaining at 21 and 22 kDa. The 21-kDa band corresponds in position to the expected location of TIMP-2. The identity of the inhibitor present at the 22-kDa location has not been established. No inhibitory activity was observed which corresponded to the location of TIMP-1 (at 28.5 kDa). Younger eyes show less inhibitory activity. The intensity of staining at 24 and 27 kDa was quantitated.

the diameter was represented by the length of atrophy measured in the tissue section. We then calculated the area of RPE atrophy and subtracted that area from 10 × 10 mm^2. With this adjusted denominator, it was apparent that the TIMP-3 content below areas where RPE is present is approximately two times higher in AMD eyes than in age-matched normal eyes (Fig. 5).

The monoclonal antibody used in this study recognized recombinant TIMP-3 in western blot analysis exhibiting characteristic 27- and 24-kDa bands. Although two higher molecular weight bands (approximately 37 and 40 kDa) appeared in the blots of most tissue samples, N-terminal amino acid sequence analysis revealed that these proteins were unrelated to TIMP-3. Reverse zymography also showed that these higher molecular weight components have no inhibitory activity. The 37-kDa nonspecific band was found to be GAPDH, a ubiquitous intracellular enzyme, and the purified protein showed cross-reactivity with the TIMP-3 antibody but with low affinity. In immunohistochemistry, however, no intracellular staining was observed. The presence of cross-reactivity in the western blot analysis and the absence of intracellular staining in immunohistochemistry probably resulted from differences in protein content. Coomassie staining of the transferred membrane showed a large amount of 37-kDa protein in the samples. The total amount of the protein in the tissue extract was large, but the concentration in each cell in the tissue sections was not sufficient to show nonspecific immunoreactivity.

Although neither structural mutations nor mutations in regulatory regions of the TIMP-3 gene are thought to be a cause of AMD,[18,19] it is possible that a mutation in a gene regulating TIMP-3 translation causes TIMP-3 elevation or that TIMP-3 change occurs downstream of other disorders—for example, changes in the ECM-binding partner. Our immunohistochemical results show that soft drusen were markedly stained with anti-TIMP-3 antibody in AMD eyes. This may imply that an elevated TIMP-3 level in the macula of AMD resulted from TIMP-3 accumulation in soft drusen. Drusen are thought to be composed of incompletely degraded debris that is exocytosed by RPE cells. Various hereditary[25–27] or nonhereditary factors such as protein alterations,[27] oxidative stress,[29–31] or disorders of hydrolytic enzymes[32,33] may participate, along with aging, in accelerating the accumulation of this debris. Those insufficiently digested materials may possess a domain with an affinity for TIMP-3 binding. Because TIMP-3 broadly inhibits MMPs, drusen with excess TIMP-3 may retard Bruch's membrane renewal. This may result in the thickening of Bruch's membrane, reducing Bruch's membrane permeability in the trafficking of metabolites and nutrients between the choroid and RPE, ultimately resulting in RPE and photoreceptor atrophy.

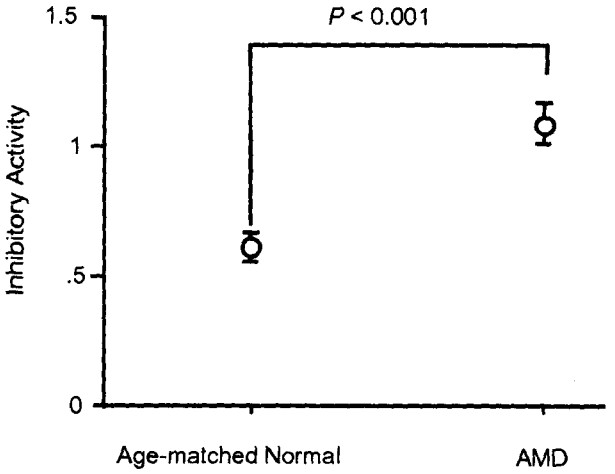

FIGURE 8. Comparison of TIMP-3 activity in the AMD and age-matched normal eyes. The inhibitory activity detected by reverse zymography was significantly elevated in AMD eyes (by approximately twofold).

In areas where choroidal neovascularization was observed, the RPE was absent, and virtually no TIMP-3 immunoreactivity was evident in the subjacent Bruch's membrane. There are two possible sequences to these changes: atrophy of the RPE leads to a decrease in TIMP-3, which is permissive to neovascularization; or choroidal neovascularization causes RPE atrophy, which is followed by TIMP-3 loss. Although current results do not indicate which occurs first, the antiangiogenic activity of TIMP-3[9,10] makes the former a more likely scenario. We speculate that, in some AMD eyes, Bruch's membrane thickening causes an atrophy of RPE, and TIMP-3 levels decrease in the area of RPE atrophy, which is permissive for choroidal neovascularization.

We conclude that the TIMP-3 content in Bruch's membrane in the macula increases during normal aging and that TIMP-3 content is elevated beyond normal levels in the macular region of AMD eyes. This suggests that TIMP-3 may be one of the key molecules causally involved in Bruch's membrane thickening during normal aging and in AMD. Further studies are needed to identify the TIMP-3 binding partner(s) in Bruch's membrane and drusen, to determine whether elevated TIMP-3 levels are caused by increased accumulation or increased synthesis of this inhibitor, and to establish whether TIMP-3 elevation is causally involved in the thickening of Bruch's membrane, which is associated with age-related macular degeneration.

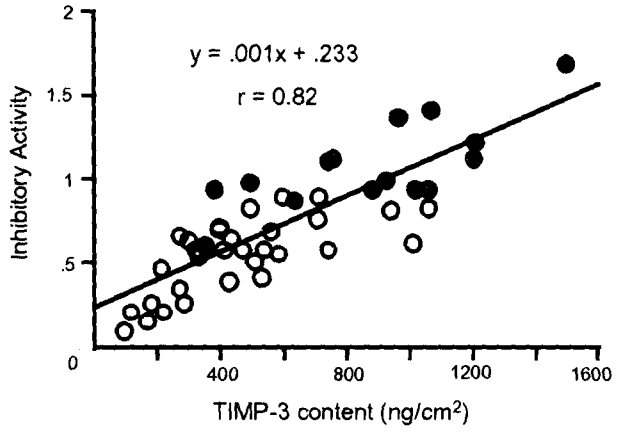

FIGURE 7. Correlation between the inhibitory activity and content of TIMP-3. The inhibitory activity in all the samples (*open circles*: normal, *closed circles*: AMD) was highly correlated with TIMP-3 content.

Acknowledgments

The authors thank Joan Fisher of The Foundation Fighting Blindness for her help in securing the AMD donor eyes used in the analysis; Jill Spitzer of the Cleveland Eye Bank for help in securing the normal eyes less than 70 years of age; and the National Disease Research Interchange for obtaining the normal eyes more than 70 years of age; Suneel Apte, Bela Anand-Apte, John W. Crabb, and Dylan R. Edwards for

valuable discussions and technical advice during the course of this study; and Mary E. Rayborn for help in proofreading the manuscript.

References

1. Birkedal-Hansen H, Moore W, Bodden M, et al. Matrix metalloproteinases: a review. *Crit Rev Oral Biol Med.* 1993;4:197-250.
2. Klagsbrun M, Folkman J. *Handbook of Experimental Pharmacology*. New York, NY: Plenum; 1990.
3. Pavloff N, Staskus P, Kishnani NS, Hawkes SP. A new inhibitor of metalloproteinases from chicken: ChIMP-3. A third member of the TIMP family. *J Biol Chem.* 1992;267:17321-17326.
4. Kishnani NS, Staskus PW, Yang TT, Masiarz FR, Hawkes SP. Identification and characterization of human tissue inhibitor of metalloproteinase-3 and detection of three additional metalloproteinase inhibitor activities in extracellular matrix. *Matrix Biol.* 1994;14:479-488.
5. Apte SS, Mattei M-G, Olsen BR. Cloning of cDNA encoding human tissue inhibitor of metalloproteinases-3 (TIMP-3) and mapping of the TIMP-3 gene to chromosome 22. *Genomics.* 1994;19:86-90.
6. Apte SS, Olsen BR, Murphy G. The gene structure of tissue inhibitor of metalloproteinases-3 (TIMP-3) and its inhibitory activities define the distinct TIMP family. *J Biol Chem.* 1995;270:14313-14318.
7. Woessner JF. Matrix metalloproteinases and their inhibitors in connective tissue remodeling. *FASEB J.* 1991;5:2145-2154.
8. Moses MA, Langer R. A metalloproteinase inhibitor as an inhibitor of neovascularization. *J Cell Biochem.* 1991;47:230-235.
9. Anand-Apte B, Bao L, Smith R, et al. A review of tissue inhibitor of metalloproteinases-3 (TIMP-3) and experimental analysis of its effect on primary tumor growth. *Biochem Cell Biol.* 1996;74:853-862.
10. Anand-Apte B, Pepper M, Voest E, et al. Inhibition of angiogenesis by tissue inhibitor of metalloproteinase-3. *Invest Ophthalmol Vis Sci.* 1997;38:817-823.
11. Leco K, Khokha R, Pavloff N, Hawkesi S, Edwards D. Tissue inhibitor of metalloproteinases-3 (TIMP-3) is an extracellular matrix-associated protein with a distinctive pattern of expression in mouse cells and tissues. *J Biol Chem.* 1994;269:9352-9360.
12. Fariss RN, Apte SS, Olsen BR, Milam AH, Iwata K. Tissue inhibitor of metalloproteinases-3 is a component of Bruch's membrane of the eye. *Am J Pathol.* 1997;150:323-328.
13. Kamei M, Apte S, Lewis H, Hollyfield JG. TIMP-3 accumulation in Bruch's membrane and drusen in eyes from normal and age-related macular degeneration donors. In: LaVail MM, Hollyfield JG, Anderson RE, eds. *Degenerative Retinal Diseases*. New York, Plenum Press; 1997:11-15.
14. Della NG, Campochiaro PA, Zack DJ. Localization of TIMP-3 mRNA expression to the retinal pigment epithelium. *Invest Ophthalmol Vis Sci.* 1996;37:1921-1924.
15. Ruiz A, Brett P, Bok D. TIMP-3 is expressed in human retinal pigment epithelium. *Biochem Biophys Res Commun.* 1996;226:467-474.
16. Weber BH, Vogt G, Pruett RC, Stohr H, Felbor U. Mutations in the tissue inhibitor of metalloproteinase-3 (TIMP-3) in patients with Sorsby's fundus dystrophy. *Nat Genet.* 1994;8:352-356.
17. Fariss RN, Apte SS, Luthert PJ, Bird AC, Milam AH. Accumulation of tissue inhibitor of metalloproteinases-3 in human eyes with Sorsby's fundus dystrophy or retinitis pigmentosa. *Br J Ophthalmol.* 1998;82:1329-1334.
18. Felbor U, Doepner D, Schneider U, Zrenner E, Weber BH. Evaluation of the gene encoding the tissue inhibitor of metalloproteinases-3 in various maculopathies. *Invest Ophthalmol Vis Sci.* 1997;38:1054-1059.
19. De La Paz MA, Pericak-Vance MA, Lennon FJLH, Seddon JM. Exclusion of TIMP-3 as a candidate locus in age-related macular degeneration. *Invest Ophthalmol Vis Sci.* 1997;38:1060-1065.
20. Piguet B, Wells J, Palmvangi I, Wormald R, Chisholm I, Bird A. Age-related Bruch's membrane change: a clinical study of the relative role of heredity and environment. *Br J Ophthalmol.* 1993;77:400-403.
21. Green WR, Enger C. Age-related macular degeneration histopathologic studies: the 1992 Lorenz E. Zimmerman Lecture. *Ophthalmology.* 1993;100:1519-1535.
22. Curcio C, Medeiros N, Millican C. The Alabama Age-Related Macular Degeneration Grading System for donor eyes. *Invest Ophthalmol Vis Sci.* 1998;39:1085-1096.
23. Yamada M, Tsukagoshii H, Otomo E, Hayakawa M. Systemic amyloid deposition in old age and dementia of Alzheimer type: the relationship of brain amyloid to other amyloid. *Acta Neuropathol.* 1988;77:136-141.
24. McFall-Ngai M, Ding L, Takemoto L, Horwitz J. Spatial and temporal mapping of the age-related changes in human lens crystallins. *Exp Eye Res.* 1985;41:745-758.
25. Heiba IM, Elston RC, Klein EK, Klein R. Sibling correlations and segregation analysis of age-related maculopathy: the Beaver Dam Eye Study. *Genet Epidemiol.* 1994;11:51-67.
26. Seddon JM, Ajani UA, Mitchell BD. Familial aggregation of age-related maculopathy. *Am J Ophthalmol.* 1997;123:199-206.
27. Allikmets R, Shroyer N, Singh N, et al. Mutation of the Stargardt disease gene (ABCR) in age-related macular degeneration. *Science.* 1997;277:1805-1807.
28. The Eye Disease Case-Control Study Group. Risk factors for neovascular age-related macular degeneration. *Arch Ophthalmol.* 1992;110:1701-1708.
29. West S, Vitale S, Halfrisch J, Munoz B, Muller D, Bressler S, Bressler N. Are antioxidants or supplements protective for age-related macular degeneration? *Arch Ophthalmol.* 1994;112:222-227.
30. Gottsch J, Bynoe L, Harlan J, Rencs E, Green W. Light-induced deposits in Bruch's membrane of protoporphyric mice. *Arch Ophthalmol.* 1993;111:126-129.
31. Hammond BR Jr, Wooten BR, Snodderly DM. Cigarette smoking and retinal carotenoids: implications for age-related macular degeneration. *Vision Res.* 1996;36:3003-3009.
32. Eldred G. Lipofuscin fluorophore inhibits lysosomal protein degradation and may cause early stages of macular degeneration. *Gerontology.* 1995;41(suppl 2):15-28.
33. Rakoczy P, Baines M, Kennedy C, Constable I. Correlation between autofluorescent debris accumulation and the presence of partially processed forms of cathepsin D in cultured retinal pigment epithelial cells challenged with rod outer segments. *Exp Eye Res.* 1996;63:159-167.

参考論文

MICROSCOPY RESEARCH AND TECHNIQUE 42:311–316 (1998)

Analysis of Extracellular Matrix Synthesis During Wound Healing of Retinal Pigment Epithelial Cells

MOTOHIRO KAMEI,[1,2]* ATSUSHI KAWASAKI,[2] AND YASUO TANO[2]
[1]*The Eye Institute, Cleveland Clinic Foundation, Cleveland, Ohio 44195 USA*
[2]*Department of Ophthalmology, Osaka University Medical School, Osaka, Japan*

KEY WORDS extracellular matrix; growth factors; immunohistochemistry; retinal pigment epithelium; wound healing

ABSTRACT To investigate changes in retinal pigment epithelial (RPE) cells during wound healing, we evaluated the deposition of newly synthesized extracellular matrix (ECM) over time during wound healing in rat RPE cultures. We also estimated the effect of growth factors on the healing rate and ECM synthesis. After preparing rat RPE cell sheet cultures, we made round 1-mm defects in the cultures. Fibronectin, laminin, and collagen IV synthesis were evaluated with immunocytochemistry every 12 hours after wounding. S-phase cell distribution was analyzed every 12 hours by 5-bromodeoxyuridine uptake. We added either platelet-derived growth factor (PDGF), epidermal growth factor (EGF), or transforming growth factor- β2 (TGF-β2) to cultures at concentrations of 1, 10, and 100 ng/mL and immunocytochemically analyzed the effects on ECM and estimated the rate of wound closure. Although approximately 50% closure was achieved 24 hours after wounding, fibronectin deposits first appeared at that time. Laminin and collagen IV were first detected at 36 hours and fibronectin staining had extended toward the wound center. S-phase cells were distributed in concentric rings that moved centripetally over time and corresponded to the leading edge of the area stained with anti-ECM antibodies. TGF-β2 enhanced ECM deposition, but EGF and PDGF did not. TGF-β2 decreased the healing rate in a dose-dependent manner, whereas PDGF promoted wound closure. EGF enhanced closure at the highest concentration only. In summary, wound healing in RPE may be initiated when cells at the wound edge slide or migrate toward the wound center, which is followed by cell proliferation and then ECM synthesis. ECM components may be produced in a specific sequence during healing. TGF-β2 may promote RPE cell differentiation, and PDGF may enhance proliferation during wound healing of the RPE. *Microsc. Res. Tech. 42:311–316, 1998.*

INTRODUCTION

Age-related macular degeneration (AMD) is the leading cause of irreversible severe visual loss in people over the age of 50 in the Western hemisphere (Bressler et al., 1988). Recent advances in vitreous surgery have made it possible to treat submacular disorders, including subretinal neovascularization and submacular hemorrhage associated with AMD (de Juan and Machemer, 1988; Kamei et al., 1996a; Lambert et al., 1992; Thomas et al., 1992). Submacular surgery, however, causes local debridement of the retinal pigment epithelium (RPE) (Berger and Kaplan, 1992; Das et al., 1992; Grossniklaus et al., 1992; Thomas et al., 1992). Although the RPE defect is eventually healed by migration and proliferation of the RPE cells adjacent to the damaged area (Del Priore et al., 1995; Heriot and Machemer, 1992; Valentino et al., 1995), characteristics specific to the RPE are lost to some degree (Del Priore et al., 1988; Grisanti and Guidry, 1995; Hergott et al., 1989; McKechnie et al., 1988; Opas, 1991), and such damage may induce photoreceptor death and increase the incidence of recurrent neovascularization after the surgery. Therefore, repairing RPE damage may be crucial for recovery of visual function. However, little is known about changes in RPE cells during wound healing.

Basement membrane, or extracellular matrix (ECM), is important in wound healing (Choi, 1994; Herrick et al., 1992; Yamakawa et al., 1988). Most kinds of cells synthesize ECM. Retinal pigment epithelial cells produce ECM, including the ECM components fibronectin, laminin, elastin, heparan sulfate proteoglycan, and collagen types I, III, and IV in vivo and in vitro (Campochiaro et al., 1986; Li et al., 1984; Newsome et al., 1988; Turksen et al., 1984). Cytokines are one of the factors regulating gene expression in RPE cells (Ando et al., 1995; Opas and Dziak, 1989; Osusky et al., 1994). Synthesis of ECM during wound healing, however, is not well understood in RPE cells.

In this study, we investigated the deposition of newly synthesized ECM over time during wound healing in rat RPE cell sheet cultures and compared it with the distribution of proliferating cells. We also examined the influence of growth factors on the healing rate and ECM synthesis.

Contract grant sponsor: Nippon Eye Bank Association.

*Correspondence to: Motohiro Kamei, M.D., The Eye Institute (FFb 33), Cleveland Clinic Foundation, 9500 Euclid Ave., Cleveland, OH 44195 USA. E-mail: kameim@cesmtp.ccf.org

Received 27 July 1997; accepted in revised form 1 April 1998

MATERIALS AND METHODS

Retinal Pigment Epithelial Cell Sheet Culture and Wounding

This study was conducted in accordance with the Association for Research in Vision and Ophthalmology Statement for the Use of Animals in Ophthalmic and Vision Research. Sheet cultures of rat RPE cells were prepared by a procedure modified from a previously described method (Kamei et al., 1996b). Briefly, eyes from 7–10-day-old Sprague-Dawley rats were incubated in 0.1% proteinase K (Merck, Darmstadt, Germany) at 37°C for 8 minutes and then for 10 minutes in culture medium, which consisted of a mixture of equal volumes of Dulbecco's modified Eagle's medium and Ham's F-12 (both, Nikken Bio Medical Laboratory, Kyoto, Japan) supplemented with 10% fetal bovine serum (FBS; HyClone Laboratories, Logan, Utah). Then, after bisecting the whole eye posterior to the ora serrata, the sclera and choroid were peeled away from the neural retina, preserving a sheet of RPE cells attached to it. The isolated tissue composed of the neural retina and adherent RPE was placed on a culture plate with culture medium with the RPE side down. A 2-chamber plastic slide (Lab-Tek, Nunc Inc., Naperville, IL) was used as a culture plate. One hour's incubation at 37°C allowed the RPE sheet to detach spontaneously from the retina as a sheet and weakly attach to the culture plate with the apical-microvilli side up.

After the RPE sheets were incubated for 24 hours to allow adequate adhesion to the culture plates, round defects 1 mm in diameter were made by pressing a trephine on the sheet culture. One to several defects per sheet were made according to sheet size so that the defects were separated by 1 mm. Six defects were analyzed in each experiment.

Immunocytochemical Analysis of Synthesized Extracellular Matrix

To evaluate the distribution of fibronectin, laminin, and collagen IV, the cultures were examined immunocytochemically every 12 hours after wounding. After rinsing away the culture medium with phosphate-buffered saline (PBS, pH 7.4), the culture plates were filled with 50% methanol and 50% acetone and the cells were fixed for 10 minutes. The cells then were incubated overnight at 4°C with the appropriate primary antibody: monoclonal mouse anti-fibronectin antibody (MAB1940, Chemicon International, Inc., Temecula, CA), monoclonal mouse anti-laminin antibody (A2–20018, Amresco, Solon, OH), or polyclonal rabbit anti-human collagen IV antibody, which has cross-reactivity with rat (PC10760, Progen Biotechnik GmbH, Heidelberg, Germany). These primary antibodies were used at a dilution of 1:500 in 0.1 M PBS containing 3% bovine serum albumin (BSA) and 0.3% Triton X-100. After overnight incubation, all specimens were labeled with fluorescein isothiocyanate-conjugated goat anti-mouse IgG (Jackson Co., St. Louis, MO) or anti-rabbit IgG (Sigma Chemical Co., St. Louis, MO) diluted 1:1000 with the PBS-BSA solution, and the cells again were incubated at 4°C overnight. The specimens were examined under an epifluorescent microscope (BX-50, Olympus, Tokyo, Japan).

S-Phase Cell Analysis

To investigate the distribution of proliferating cells during wound healing, cells in the S-phase were identified every 12 hours using 5-bromodeoxyuridine (BrdU) incorporation and immunocytostaining. Ten μM BrdU (Sigma) was added to the culture medium 9 hours before fixation. Immunocytochemical staining using the same procedures described above was performed using monoclonal anti-BrdU antibody (Becton Dickinson Immunocytometry Systems, San Jose, CA) as the primary antibody. The nuclei were counterstained with 0.04 μg/mL propidium iodide.

Growth Factor Supplementation

After the RPE sheets were incubated in the medium with 10% FBS for 24 hours, they were rinsed twice with serum-free medium and then incubated under serum-free conditions for 24 hours to eliminate the influence of growth elements in the serum. Then 1-mm round defects were made in the sheet, the medium was replaced with medium supplemented with 0.1% FBS, and one of the three following recombinant human growth factors was added: platelet-derived growth factor-BB (PDGF-BB; Genzyme, Cambridge, MA), epidermal growth factor (EGF; Toyobo, Osaka, Japan), or transforming growth factor- β2 (TGF-β2; Genzyme). These growth factors were applied at concentrations of 1, 10, and 100 ng/mL. For controls, RPE sheets were treated in the same way, but no growth factors were added. Immunocytochemistry was performed for the ECM as described above and the rate of wound closure was estimated.

Rate of Wound Closure

Phase-contrast micrographs were taken every 8 hours after wound formation and the area of wound remaining was measured using a computerized area analyzer (Micro Computer Imaging Device, Imaging Research Inc., Ontario, Canada). The ratio of the wound area remaining was compared to the initial 1-mm wound area to evaluate the rate of wound healing.

Statistical Analysis

The wound healing rate with each growth factor at each concentration was compared with controls and the effects were analyzed by using two-way repeated-measures ANOVA. Significance was accepted at $P < 0.05$.

RESULTS

Deposition of Extracellular Matrix and Distribution of S-Phase Cells Over Time

Although approximately 50% closure was achieved 24 hours after wounding and complete closure achieved at 48 hours (Fig. 1, column 1), fibronectin deposits were first apparent at 24 hours (Fig. 1, column 3), and laminin and collagen IV were detected at 36 hours (data not shown). At 48 hours, fibronectin staining (Fig. 1, column 3) occurred more centrally than laminin and collagen IV staining (Fig. 1, columns 4 and 5). Fibronectin was detected only in the area covered with regenerated RPE cells, whereas laminin and collagen IV were present in both wounded and unwounded areas. The entire wound area except a central zone was covered

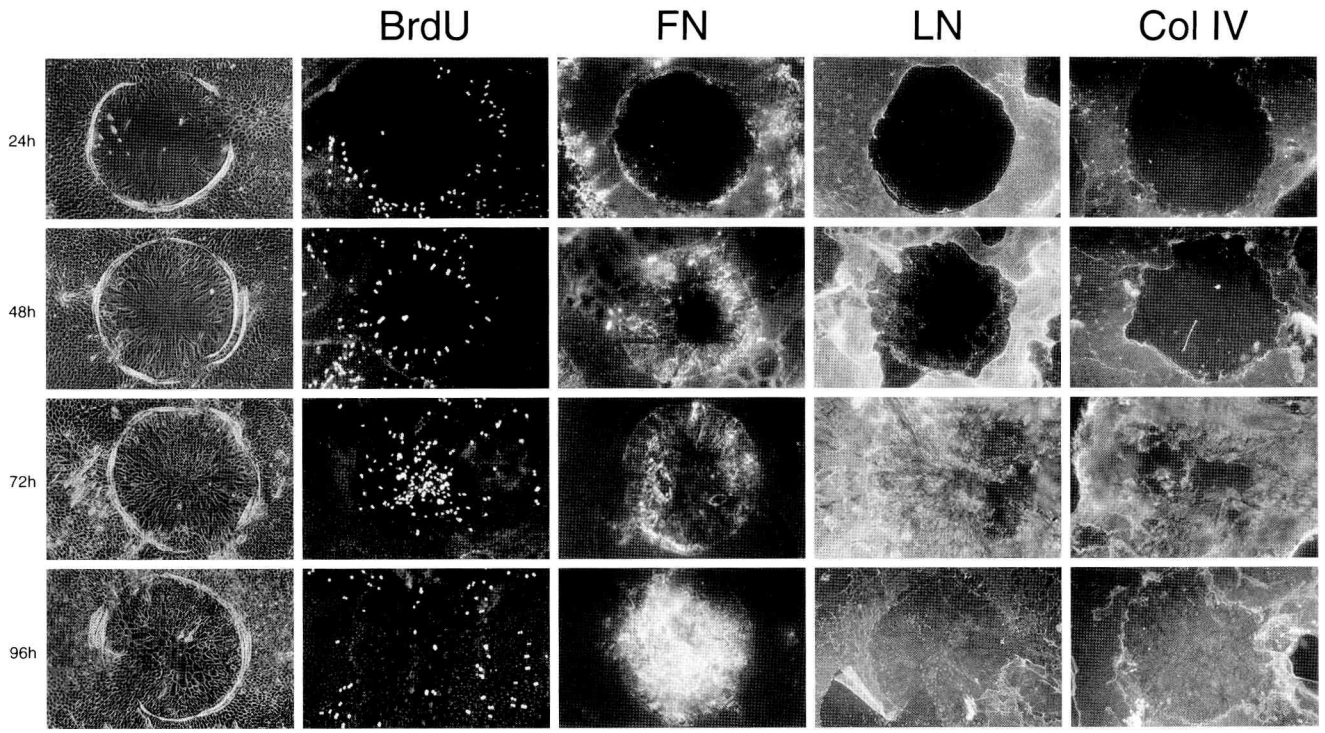

Fig. 1. First column: Phase-contrast photomicrographs of the wounds in RPE cell sheet cultures 24, 48, 72, and 96 hours after wounding. Approximately 50% closure was achieved at 24 hours. The defect was completely covered with migrating and proliferating cells at 48 hours although the cells were spindle-shaped. The cell population became denser and the cells became more polygonal over time. Second column: Micrographs of RPE cells in the wound stained for anti-BrdU antibody. S-phase cells that showed positive signals were first recognised at 24 hours as a circle at the peripheral zone of the wound and then moved centripetally, forming concentric circles over time after wounding. Few nuclei stained at 96 hours; those that did were scattered uniformly over the sheet. Third through fifth columns: Immunofluorescent micrographs of the wounds stained with anti-fibronectin (FN, 3rd column), laminin (LN, 4th column), and collagen VI (Col IV, 5th column) antibody. Fibronectin was first observed at 24 hours, but laminin and collagen VI were not stained yet. Laminin and collagen IV staining was recognised 48 hours after wounding and, at that time, fibronectin staining occurred more centrally than other ECM staining. The entire wound area except a central zone is covered with deposits of these ECM components at 72 hours and completely covered at 96 hours. Distribution of BrdU staining (2nd column) corresponded to the leading edge of the area staining positively for ECM. Original magnification, 10x.

with deposits of these ECM components at 72 hours (Fig. 1, columns 3–5). Fibronectin stained in a filament-like manner, and collagen IV and laminin stained diffusely. It took 96 hours for these ECM constituents to accumulate over the entire wound area.

Anti-BrdU antibody staining revealed S-phase cells that formed concentric circles according to the time elapsed since wounding (Fig. 1, column 2). The first circle to appear was the largest, located at the peripheral zone of the wound at 24 hours after wounding; subsequently, smaller circles appeared centripetally. At 84 hours, the innermost circles were located at the center of the wound as a cluster (data not shown) and this BrdU-positive zone corresponded to the leading edge of the area staining positively for ECM (Fig. 1, columns 3–5). Few additional nuclei stained at 96 hours, and those that did were scattered uniformly over the sheet. Consequently, cell proliferation to repair wounds 1 mm in diameter ceased by 96 hours after wounding.

Effect of Growth Factors on ECM Deposition and Healing Rate

TGF-β2 remarkably enhanced deposition of fibronectin (Fig. 2A), laminin, and collagen IV (data not shown) when compared with a control sheet (Fig. 2D) under an epifluorescent microscope, whereas cultures supplemented with PDGF or EGF (Fig. 2B,C) did not show an apparent increase in deposition of these ECM components. Cultures incubated with EGF or PDGF showed a filamentous pattern of deposition that differed from the control and TGF-β2-supplemented cultures.

Compared to controls, TGF-β2 decreased the healing rate at all three concentrations ($P = 0.03, 0.003, 0.0003$ at 1, 10, 100 ng/mL, respectively), whereas PDGF promoted wound closure at concentrations of 10 and 100 ng/mL ($P = 0.77, 0.002, 0.002$ at 1, 10, 100 ng/mL, respectively) (Fig. 3). The healing rate was not significantly affected at EGF concentrations of 1 and 10 ng/mL but was enhanced at 100 ng/mL ($P = 0.72, 0.69, 0.02$ at 1, 10, 100 ng/mL, respectively).

DISCUSSION

This study revealed a time lag between ECM deposition and wound closure. Wound healing may be initiated when cells at the wound edge slide or migrate toward the center of a round defect, which is followed by cell proliferation and then synthesis of ECM.

We observed BrdU-positive S-phase cells at 24 hours but not at 12 hours after wounding, although we

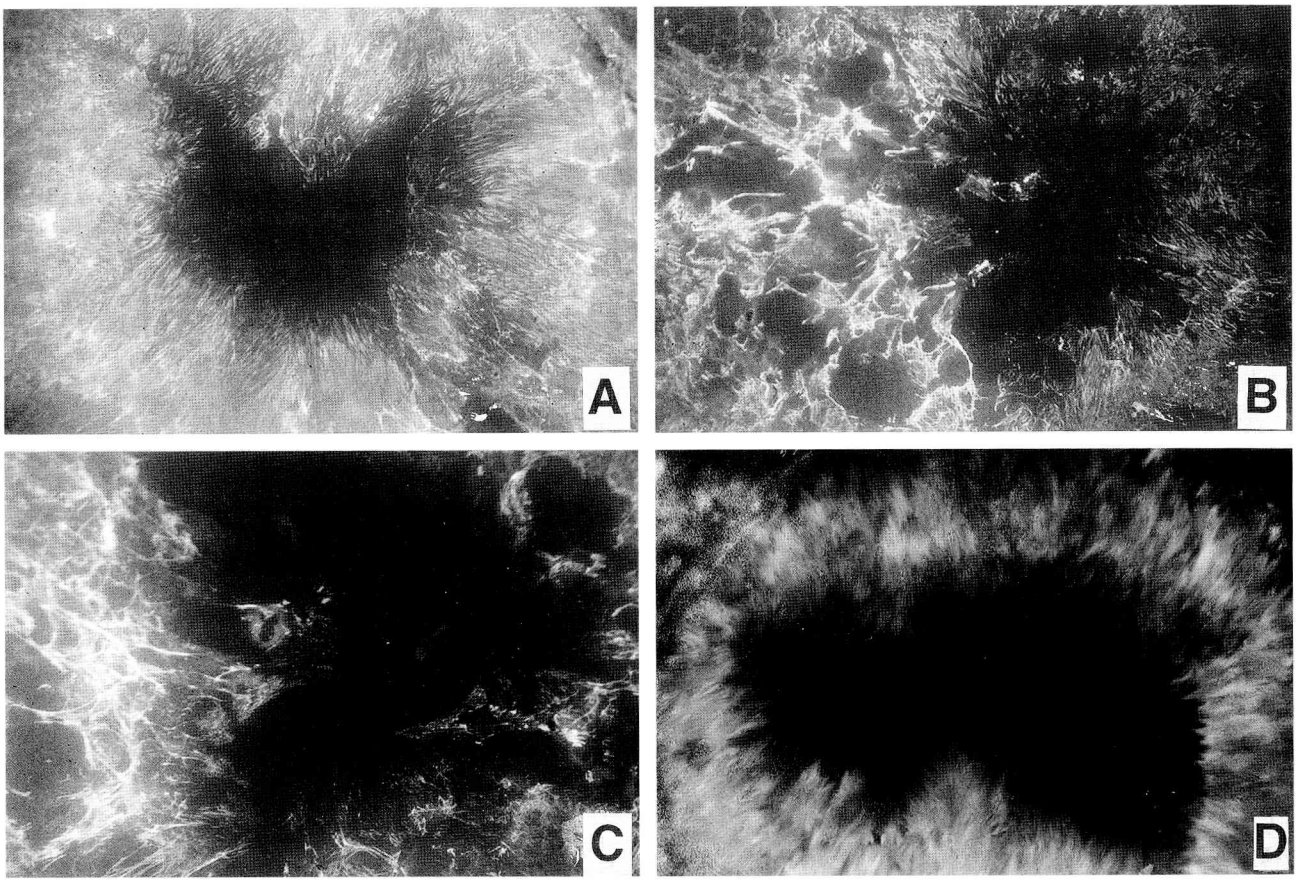

Fig. 2. Epifluorescent micrographs of the wound stained with anti-fibronectin antibody 60 hours after wounding. TGF-β2 added in the culture medium (**A**) appears to enhance deposition of fibronectin when compared with the no-treatment control (**D**). Cultures incubated with PDGF (**B**) or EGF (**C**) show a filamentous pattern of deposit that differs from the control and TGF-β2-supplemented cultures. Original magnification, 20x.

previously reported (Kamei et al., 1996b) in the same wound healing model that about 20% of closure is obtained at 12 hours after wounding. This finding suggests that cell spreading or sliding from the wound edge accomplishes the initial 20% of wound closure without proliferation. Considering that a circle 900 μm in diameter corresponds to 81% of a 1-mm round defect, an initial 20% wound closure at 12 hours means that an approximate 50-μm wide peripheral zone is covered with spreading cells. We thus can say that cells covering an approximate 50-μm wide peripheral zone at 12 hours had not yet proliferated. This observation is consistent with a previous report using organ culture and proliferating cell nuclear antigen (PCNA) staining that found RPE cells in wounds narrower than 125 ± 48 μm did not express PCNA (Hergott and Kalnins, 1991). Thus, the process of wound healing may be initiated by cell sliding or migration at the wound edge; cell proliferation then follows.

A BrdU-positive signal observed as a ring near the wound edge at 24 hours moved centripetally, forming concentric circles until 84 hours. ECM staining did not occur centrally beyond these concentric BrdU-positive circle at any time point. In other words, the BrdU-positive zone constituted the leading edges of ECM deposits. Thus, ECM synthesis may follow cell proliferation during RPE wound healing, but studies of mRNA expression that include in situ hybridization are needed to confirm this observation.

Fibronectin synthesis preceded that of laminin and collagen IV. Deposits of fibronectin were first apparent at 24 hours after wounding, and laminin and collagen IV were first seen at the peripheral zone of the wound at 36 hours when fibronectin staining had begun to extend toward the center of the wound. This sequence of events suggests that ECM components are produced in a certain order during wound healing.

We selected the TGF-β2, PDGF, and EGF cytokines for several reasons. TGF-β upregulates the synthesis of ECM components in the RPE (Ando et al., 1995; Osusky et al., 1994) and many other kinds of cells (Ignotz and Massague, 1986; Vollberg et al., 1991), and it is the only growth factor that inhibits cell proliferation under in vitro conditions (Massague, 1990) and that is clinically applied in macular hole surgery as a promotor of wound healing in RPE or glial cells (Glaser, 1992). As an autocrine stimulator of growth in RPE, PDGF may play an essential role in retinal wound repair (Campochiaro et al., 1994). EGF enhances wound healing in various types of epithelial cells, including RPE cells (Leschey et al., 1990), and clinically is applied to persistent corneal ulcer (Scardovi et al., 1993). Although the growth factors used in this study were recombinant human proteins, we decided to apply them to rat cells because a

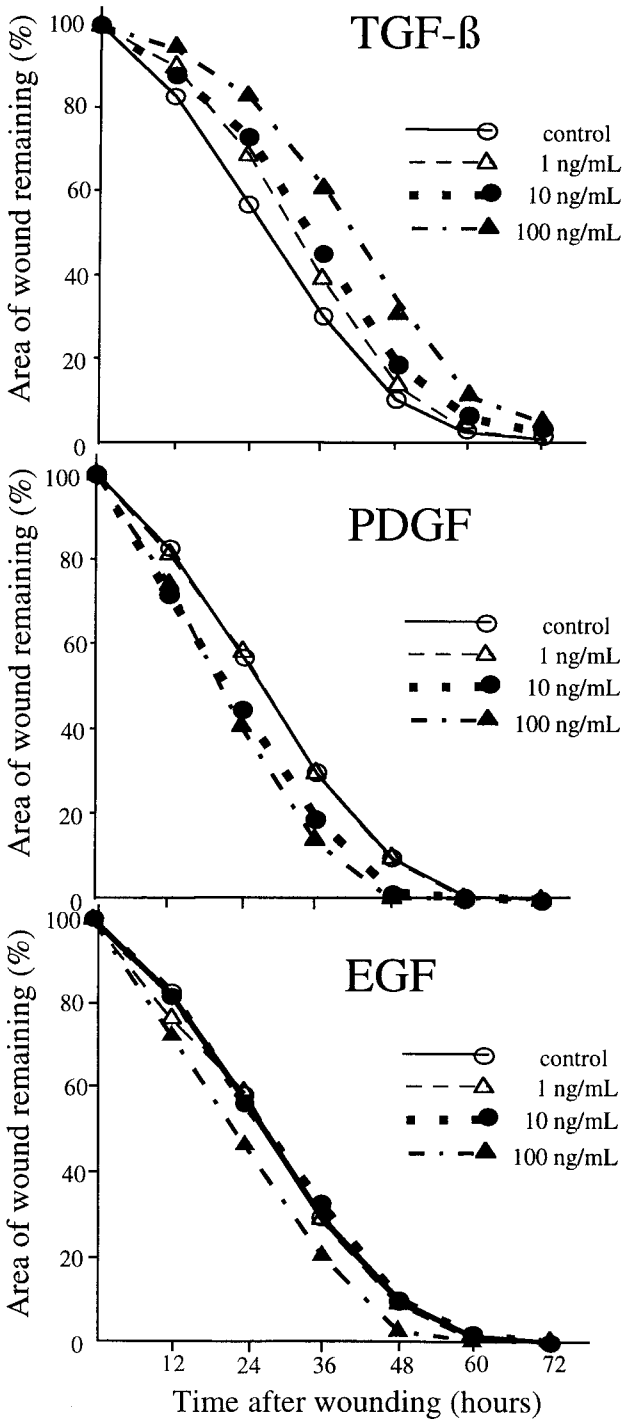

Fig. 3. Wound closure rate in the retinal epithelial cell sheet cultures incubated with various kinds and doses of growth factors. Compared to control cells (no growth factor added), TGF-β2 decreased the healing rate at all three concentrations, whereas PDGF promoted wound closure at concentrations of 10 and 100 ng/mL. EGF enhanced closure only at 100 ng/mL.

previous report demonstrated the efficacy of human cytokines (including TGF-β, PDGF, EGF, HGF, IGF, and VEGF) on rat culture cells (Nicosia et al., 1994).

In our RPE wound-healing model, TGF-β2 appeared to enhance deposition of ECM instead of decreasing the healing rate. This result is consistent with previous studies that report that TGF-β upregulates the synthesis of ECM components and inhibits cell proliferation in vitro. In contrast to TGF-β2 and controls, both PDGF and EGF produced fibronectin deposits in a filamentous pattern and did not increase ECM deposition, but did promote wound closure.

In conclusion, these findings suggest that TGF-β2 promotes differentiation of RPE cells, and PDGF enhances their proliferation during wound healing of the RPE. Quantitative analysis of ECM deposition and proliferating cells is required to establish the validity of this mechanism.

ACKNOWLEDGMENTS

We are indebted to Dr. Atsushi Hayashi for valuable advice on the experimental design and technique, Michelle Secic for statistical analysis, and Cassandra Talerico for manuscript preparation.

REFERENCES

Ando, H., Kodama, R., Tomoda, Y., and Eguchi, G. (1995) Transforming growth factor-β1 induces morphological changes accomplished by extracellular matrix reconstitution in cultures of avian retinal pigmented epithelial cells. Jpn. J. Ophthalmol., 39:1–11.

Berger, A.S., and Kaplan, H.J. (1992) Clinical experience with the surgical removal of subfoveal neovascular membranes. Ophthalmology 99:969–976.

Bressler, N.M., Bressler, S.B., and Fine, S.L. (1988) Age-related macular degeneration. Surv. Ophthalmol., 32:375–413.

Campochiaro, P.A., Jerdan, J.A., and Glaser, B.M. (1986) The extracellular matrix of human retinal pigment epithelial cells in vivo and its synthesis in vitro. Invest. Ophthalmol. Vis. Sci., 27:1615–1621.

Campochiaro, P.A., Hackett, S.F., Vinores, S.A., Freund, J., Csaky, C., LaRochelle, W., Henderer, J., Johnson, M., Rodriguez, I.R., Friedman, Z., Derevjanik, N., and Dooner, J. (1994) Platelet-derived growth factor is an autocrine growth stimulator in retinal pigmented epithelial cells. J. Cell Sci., 107:2459–2469.

Choi, B.E. (1994) Role of basement membrane in neurogenesis and repair of injury in the central nervous system. Microsc. Res. Tech., 28:193–203.

Das, A., Puklin, J.E., Frank, R.N., and Zhang N.L. (1992) Ultrastructural and immunocytochemistry of subretinal neovascular membranes in age-related macular degeneration. Ophthalmology 99: 1368–1376.

de Juan, E. Jr., and Machemer, R. (1988) Vitreous surgery for hemorrhagic and fibrous complications of age-related macular degeneration. Am. J. Ophthalmol., 105:25–29.

Del Priore, L.V., Glaser, B.M., Quigley, H.A., Dorman, M.E., and Green, W.R. (1988) Morphology of pig retinal pigment epithelium maintained in organ culture. Arch. Ophthalmol., 106:1286–1290.

Del Priore, L.V., Hornbeck, R., Kaplan, H.J., Jones, Z., Valentino, T.L., Mosinger-Ogilvie, J., and Swinn, M. (1995) Debridement of the pig retinal pigment epithelium in vivo. Arch. Ophthalmol., 113:939–944.

Glaser, B.M. (1992) Transforming growth factor-beta 2 for the treatment of full-thickness macular holes. A prospective randomized study. Ophthalmology, 99:1162–1173.

Grisanti, S., and Guidry, C. (1995) Transdifferentiation of retinal pigment epithelial cells from epithelial to mesenchymal phenotype. Invest. Ophthalmol. Vis. Sci., 36:391–405.

Grossniklaus, H.E., Martinez, J.A., and Brown, V.B. (1992) Immunocytochemical properties of surgically excised neovascular membranes in age-related macular degeneration. Am. J. Ophthalmol., 114:464–472.

Hergott, G.J., and Kalnins, V.I. (1991) Expression of proliferating cell nuclear antigen in migrating retinal pigment epithelial cells during wound healing in organ culture. Exp. Cell Res., 195:307–314.

Hergott, G.J., Sandig, M., and Kalnins, V.I. (1989) Cytoskeletal organization of migrating retinal pigment epithelial cells during wound healing in organ culture. Cell Motil. Cytoskeleton, 13:83–93.

Heriot, W.J., and Machemer, R. (1992) Pigment epithelial repair. Graefes Arch. Clin. Exp. Ophthalmol., 230:91–100.

Herrick, S.E., Sloan, P., McGurk, M., Freak, L., McClollum, C.N., and Ferguson, M.W.J. (1992) Sequential changes in histologic pattern and extracellular matrix deposition during the healing of chronic venous ulcers. Am. J. Pathol., 141:1085–1095.

Ignotz, R.A., and Massague, J. (1986) Transforming growth factor-β stimulates the expression of fibronectin and collagen and their incorporation into the extracellular matrix. J. Biol. Chem., 261:4337–4345.

Kamei, M., Tano, Y., Maeno, T., Ikuno, Y., Mitsuda, H., and Yuasa, T. (1996a) Surgical removal of submacular hemorrhage using tissue plasminogen activator and perfluorocarbon liquid. Am. J. Ophthalmol., 121:276–275.

Kamei, M., Lewis, J.M., Hayashi, A., Sakagami, K., Ohji, M., and Tano, Y. (1996b) A new wound healing model of retinal pigment epithelial cells in sheet culture. Curr. Eye Res., 15:714–718.

Lambert, H.M., Capone, A. Jr., Aaberg, T.M., Sternberg, P. Jr., Mandell, B.A., and Lopez, P.F. (1992) Surgical excision of subfoveal neovascular membranes in age-related macular degeneration. Am. J. Ophthalmol., 113:257–262.

Leschey, K.H., Hackett, S.F., Singer, J, and Campochiaro, P.A. (1990) Growth factor responsiveness of human retinal pigment epithelial cells. Invest. Ophthalmol. Vis. Sci., 31:839–847.

Li, W., Stramm, L.E., Aguirre, G.D., and Rockey, J.H. (1984) Extracellular matrix production by cat retinal pigment epithelium in vitro: Characterization of type IV collagen synthesis. Exp. Eye Res., 38:291–304.

Massague, J. (1990) The transforming growth factor-β family. Annu. Rev. Cell Biol., 6:597–641.

McKechnie, N.M., Boulton, M., Robey, H.L., Savage, F.J., and Grierson, I. (1988) The cytoskeletal elements of human retinal pigment epithelium: In vitro and in vivo. J. Cell Sci., 91:303–312.

Newsome, D.A., Pfeffer, B.A., Hewitt, A.T., Robey, P.G., and Hassell, J.R. (1988) Detection of extracellular matrix molecules synthesized in vitro by monkey and human retinal pigment epithelium: Influence of donor age and multiple passages. Exp. Eye Res., 46:305–321.

Nicosia, R.F., Nicosia, S.V., and Smith, M. (1994) Vascular endothelial growth factor, platelet-derived growth factor, and insulin-like growth factor-1 promote rat aortic angiogenesis in vitro. Am. J. Pathol., 145:1023–1029.

Opas, M. (1991) Expression of the differentiated phenotype by epithelial cells in vitro is regulated by both biochemistry and mechanics of the substratum. Dev. Biol., 131:281–293.

Opas, M., and Dziak, E. (1989) Effect of TGF-beta on retinal pigmented epithelium in vitro. Exp. Cell Biol., 57:206–212.

Osusky, R., Soriano, D., Ye, J., and Ryan, S.J. (1994) Cytokine effect on fibronectin release by retinal pigment epithelial cells. Curr. Eye Res., 13:569–574.

Scardovi, C., De Felice, G.P., and Gazzaniga, A. (1993) Epidermal growth factor in the topical treatment of traumatic corneal ulcers. Ophthalmologica, 206:119–124.

Thomas, M.A., Grand, M.G., Williams, D.F., Lee, C.M., Pesin, S.R., and Lowe, M.A. (1992) Surgical management of subfoveal choroidal neovascularization. Ophthalmology, 99:952–968.

Turksen, K., Aubin, J.E., Sodek, J., and Kalnins, V.I. (1984) Changes in the distribution of laminin, fibronectin, type VI collagen and heparan sulfate proteoglycan during colony formation by chick retinal pigment epithelial cells in vitro. Coll. Rel. Res., 4:413–426.

Valentino, T.L., Kaplan, H.J., Del Priore, L.V., Fang, S.R., Berger, A., and Silverman, M.S. (1995) Retinal pigment epithelial repopulation in monkeys after submacular surgery. Arch. Ophthalmol., 113:932–938.

Vollberg, T.M. Sr., George M.D., and Jetten, A.M. (1991) Induction of extracellular matrix gene expression in normal human keratinocytes by transforming growth factor-β is altered by cellular differentiation. Exp. Cell Res., 193:93–100.

Yamakawa, R., Shirakawa, H., Yoshimura, N., Okada, M., Asayama, K., Matsumura, M., and Ogino, N. (1988) Involvement of fibronectin in vivo regeneration of retinal pigment epithelium. Graefes Arch. Clin. Exp. Ophthalmol., 226:11–14.

参考論文

Surgical Removal of Submacular Hemorrhage Using Tissue Plasminogen Activator and Perfluorocarbon Liquid

MOTOHIRO KAMEI, M.D., YASUO TANO, M.D., TAKATOSHI MAENO, M.D., YASUSHI IKUNO, M.D., HISATOSHI MITSUDA, M.D., AND TAKENOSUKE YUASA, M.D.

• PURPOSE: To assess the result of surgical removal of submacular hemorrhage by using tissue plasminogen activator and perfluorocarbon liquid.

• METHODS: In 22 consecutive patients (22 eyes), subretinal hemorrhage associated with age-related macular degeneration, which involved the fovea and completely obscured the choroidal vascular pattern, was treated by pars plana vitrectomy. The hemorrhages were liquefied with tissue plasminogen activator, squeezed into the vitreous cavity with perfluorocarbon liquid, and then evacuated.

• RESULTS: Efficacy of the procedure was judged by the best postoperative corrected visual acuity, which was 20/100 or better in 16 eyes (73%). Submacular hemorrhage recurred in four (18%) eyes, epiretinal membrane formed in three (14%) eyes, and retinal detachment occurred in three (14%) eyes. Best-corrected final visual acuity was improved postoperatively in 18 (82%) of the 22 eyes, unchanged in three (14%) eyes, and decreased in one (5%) eye. Final visual acuity was 20/200 or better in 15 eyes (68%) and limited in other eyes by subretinal hemorrhage of greater than 30 days' duration or subfoveal neovascularizations.

• CONCLUSIONS: Use of tissue plasminogen activator and perfluorocarbon liquid in surgical removal of submacular hemorrhage may improve the outcome of surgery by reducing surgically induced retinal damage.

Accepted for publication Aug. 3, 1995.

From the Department of Ophthalmology, Osaka University Medical School (Drs. Kamei, Tano, and Maeno); and Department of Ophthalmology, Osaka National Hospital (Drs. Ikuno, Mitsuda, and Yuasa), Osaka, Japan.

Reprint requests to Motohiro Kamei, M.D., Department of Ophthalmology, Osaka University Medical School, 2-2 Yamadaoka, SUITA 565, Japan; fax: 81-6-879-3458.

SUBMACULAR HEMORRHAGE, PARTICULARLY IF THE hemorrhage is thick or associated with age-related macular degeneration, can cause severe visual loss.[1] Although recent advances in vitreous surgery have made it possible to remove subretinal hemorrhage,[2-5] procedures resulted in limited recovery of vision. Fibrin begins to form an hour after experimentally created subretinal hemorrhage,[6] and by the time patients undergo surgery to treat subretinal hemorrhage, the fibrin network that has formed cannot be aspirated. As a result, surgery to remove these coagulated hemorrhages has usually involved a large retinotomy, subretinal insertion of instruments, such as an extrusion needle, or active suction at the subretinal space. This technique poses risk of trauma to the retina, which may account for the disappointing results of such surgery to date.

Fibrinolysis with tissue plasminogen activator has been shown to enhance the clearance of experimental subretinal hemorrhage in animals.[7,8] Tissue plasminogen activator has also been used as an alternative or adjunct to surgical removal of subretinal hemorrhage,[7-11] although procedures in which it is used are controversial.[10] Even in the one study that reported the use of tissue plasminogen activator to be effective in removing subretinal hemorrhage,[9] the

procedure was successful in restoring vision to satisfactory levels only in a minority of patients.

We hypothesized that trauma to the neurosensory retina and retinal pigment epithelium during manipulation to remove subretinal hemorrhage plays an important role in the failure of surgery, even techniques that use tissue plasminogen activator, to improve vision. Perfluorocarbon liquid has been used in submacular surgery to assist in expression of liquefied subretinal hemorrhage[11] or to block possible bleeding immediately after excision of a subfoveal neovascular membrane.[12] Thus, we studied a procedure using perfluorocarbon liquid as well as tissue plasminogen activator and a technique designed to minimize retinal trauma.

PATIENTS AND METHODS

CANDIDATES FOR THIS STUDY WERE PATIENTS WITH submacular hemorrhage associated with age-related macular degeneration that involved a zone of at least one disk diameter centered at the foveola, localized mainly between the neurosensory retina and retinal pigment epithelium. In all cases, the hemorrhage was thick enough to cause an obvious elevation of the fovea and to completely obscure the choroidal vascular pattern under the hemorrhage. Contraindications to participation in the study included the following conditions: (1) subretinal hemorrhage, regardless of size, that did not involve the macula; (2) submacular hemorrhage thin enough that the choroidal vascular pattern could be seen at the macula; (3) hemorrhage mainly beneath the retinal pigment epithelium; or (4) completely organized hemorrhage (appearing as white-yellow clots). The risks and possible benefits of the procedure were explained in detail to all candidates, and those who gave written consent to the procedure were operated on.

Between July 1992 and August 1994, 22 consecutive patients underwent pars plana vitrectomy and transvitreal drainage of submacular hemorrhage at Osaka National Hospital, Osaka, Japan. The preoperative ophthalmic examination included determination of best-corrected visual acuity, slit-lamp examination, indirect ophthalmoscopy, analysis of visual fields, and fluorescein angiography. Fundus photographs were taken, and the area of submacular hemorrhage was determined from the photographs.

The average age of the eight women and 14 men in the study was 68.0 years (range, 46 to 85 years). The mean duration of visual loss before surgery was 23.0 days (range, five to 100 days), and the average area of submacular hemorrhage was 25.5 disk areas (range, one to 100 disk areas). Two of the 22 patients had previously undergone laser photocoagulation to subretinal neovascularization in the parafoveal area.

Postoperatively, patients underwent the same examination as preoperatively, under the same conditions. Best-corrected visual acuity was examined by a technician who was masked to the surgical procedure. We assessed two kinds of postoperative best-corrected visual acuity: the best visual acuity occurring during the postoperative follow-up period and the final visual acuity at the end of the follow-up period. Differences between preoperative and postoperative visual acuities and the following factors were analyzed by using Fisher's exact test: age, gender, duration of submacular hemorrhage, area of submacular hemorrhage, presence of hemorrhagic pigment epithelial detachment, and persistence of subretinal neovascularization. Postoperative complications were also recorded and evaluated.

Figure 1 shows the steps in the operative procedure. A three-port pars plana vitrectomy was performed, and the posterior hyaloid membrane was removed carefully. The flattened and bent tip of a 27- or 30-gauge blunt needle was inserted into the subretinal hemorrhage at its superotemporal edge without previous retinotomy or endodiathermy. Tissue plasminogen activator (25 μg/0.1 ml of balanced saline solution, a dose determined not to cause retinal toxicity when injected into the subretinal space in animals[7]) was gently injected until it covered the submacular hemorrhage. The total volume of injected tissue plasminogen activator ranged between 0.05 and 0.20 ml, depending on the volume of the submacular hemorrhage.

After a 20-minute wait for fibrinolysis to occur, vitreoretinal scissors were used to make a retinotomy about 1 mm long at the injection site (endodiathermy was applied before retinotomy in the first 17 eyes). Perfluorocarbon liquid (perfluoro-n-octane or perfluorodecalin) was injected onto the inferonasal retina

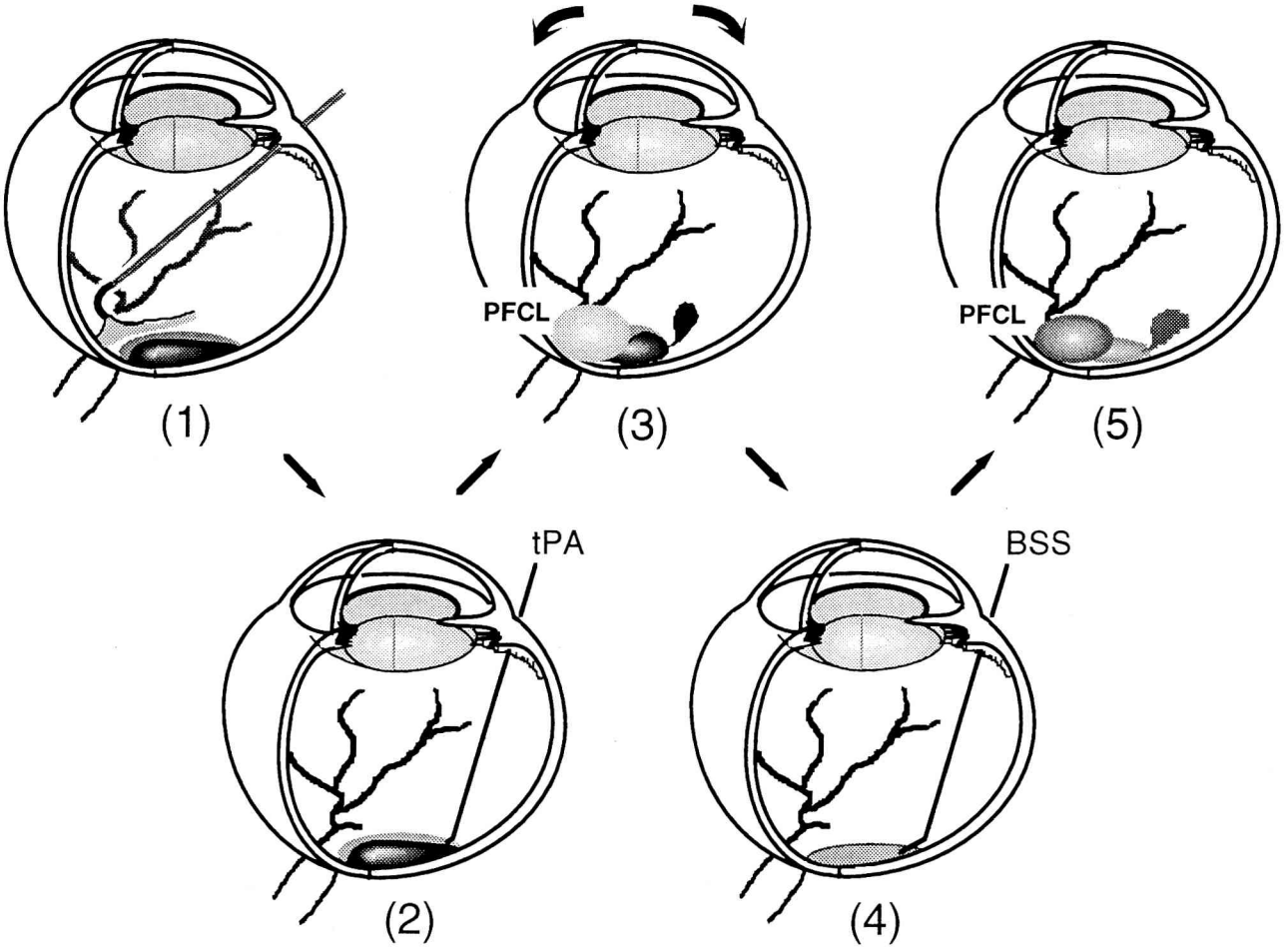

Fig. 1 (Kamei and associates). Surgical procedure. (1) Vitrectomy and careful removal of the posterior hyaloid membrane with a silicone-tipped needle. (2) Without retinotomy, the retina is perforated, and tissue plasminogen activator (tPA) is injected subretinally with a 27-gauge blunt needle. (3) Perfluorocarbon liquid (PFCL) is dropped onto the retina, and the submacular hemorrhage is squeezed into the vitreous cavity by gently rocking the eye from side to side. (4) Balanced saline solution (BSS) is injected into the subretinal space to dilute fibrin degradation products. (5) Perfluorocarbon liquid (PFCL) is applied again. After fluid-air exchange, the operation is concluded with injection of expanding gas.

until it reached the retinotomy. The submacular hemorrhage was then squeezed into the vitreous cavity through the retinotomy by applying a rocking motion to the eye. The hemorrhage drained into the vitreous cavity and was aspirated.

Balanced saline solution was gently injected into the subretinal space to dilute and flush out the fibrin degradation products, which have strong chemotactic and inflammatory properties. After a second administration of liquid perfluorocarbon and manipulation to squeeze out the fibrin degradation products, a fluid-air exchange was performed. The operation was concluded with infusion of 15% to 20% SF_6 gas (endophotocoagulation was performed around the retinotomy in the first 17 eyes).

RESULTS

PATIENT FOLLOW-UP RANGED FROM SEVEN TO 31 months after the last surgery for submacular hemorrhage (mean ± S.D., 15 ± 7 months) (Table).

In two eyes (Patients 5 and 20), peripheral retinal detachment occurred intraoperatively but was suc-

TABLE

PREOPERATIVE AND POSTOPERATIVE PATIENT DATA

PATIENT NO., AGE (YRS), GENDER	FOLLOW-UP TIME (MOS)	AREA OF SUBRETINAL HEMORRHAGE (DISK AREAS)	DURATION OF SUBRETINAL HEMORRHAGE (DAYS)	SUBRETINAL PIGMENT EPITHELIAL HEMORRHAGE	BEST-CORRECTED VISUAL ACUITY			POSTOPERATIVE DETECTION OF SUBRETINAL NEOVASCULARIZATION	POSTOPERATIVE COMPLICATIONS
					PREOPERATIVE*	POSTOPERATIVE			
						BEST	FINAL		
1, 63, M	31	10	8	No	20/800	20/60	20/200	Subfovea	Recurrence
2, 69, F	30	9	5	Yes	20/100	20/30	20/30	Extrafovea	
3, 85, M	27 (21)†	20	5	Yes	20/250	20/60	20/400	Subfovea	Recurrence
4, 78, F	24	49	30	No	HM	20/250	20/250	Extrafovea	Retinal detachment
5, 68, M	23	28	15	No	20/600	20/60	20/200	Subfovea	
6, 48, M	22	10	5	No	20/300	20/40	20/40	Extrafovea	Recurrence
7, 51, F	22	21	11	Yes	CF	20/50	20/50	Juxtafovea	
8, 69, F	17	8	10	No	20/100	20/25	20/25	None	
9, 46, F	15	100	20	Yes	HM	20/25	20/25	None	Retinal detachment, epiretinal membrane
10, 78, M	14	12	18	No	CF	20/300	20/400	Subfovea	
11, 73, F	14	9	8	No	20/800	20/30	20/40	None	
12, 67, M	14	32	85	No	20/200	20/200	20/250	Subfovea	
13, 74, M	13	6	5	Yes	20/100	20/25	20/25	Juxtafovea	
14, 67, F	11 (7)†	100	13	Yes	LP	20/100	20/200	Juxtafovea	Recurrence, retinal detachment
15, 69, F	11	39	6	Yes	20/500	20/100	20/125	Juxtafovea	Epiretinal membrane
16, 84, M	10	3	7	No	20/300	20/60	20/80	None	
17, 68, M	10	1	13	No	20/300	20/250	20/250	Subfovea	Epiretinal membrane
18, 66, M	8	9	25	No	20/800	20/80	20/100	Juxtafovea	
19, 73, M	8	20	21	Yes	20/600	20/50	20/60	None	
20, 64, M	7	28	90	No	20/500	20/250	20/250	None	
21, 78, M	7	12	100	No	20/500	20/400	20/600	Subfovea	
22, 57, M	7	54	7	Yes	20/100	20/20	20/25	None	

*CF indicates counting fingers; HM, hand motions; and LP, light perception.
†Follow-up time (months) after last vitrectomy.

cessfully treated with scleral buckling at the time of surgery. By the end of the procedure, the submacular hemorrhage was noticeably thinner in all eyes. In ten eyes (45%), the pattern of choroidal vessels could be recognized through the residual hemorrhage at the macula. By three months after surgery, almost all unorganized hemorrhage had been absorbed, but organized hemorrhage (appearing white-yellow at the time of surgery) was not liquefied by application of tissue plasminogen activator and was absorbed six to nine months after surgery.

The best visual acuity attained postoperatively was used to measure the efficacy of the procedure. Visual acuity improved postoperatively by two or more Snellen visual acuity lines in 19 (86%) of the 22 eyes and remained within one Snellen line in three eyes (14%). No patient showed a decrease between preoperative and best postoperative visual acuity. Best postoperative visual acuity was 20/100 or better in 16 (73%) of the 22 eyes.

Four eyes (18%) had relatively good visual acuity (20/100) preoperatively and had best postoperative

visual acuity of 20/30 or better. Thirteen (59%) of the 22 eyes had preoperative visual acuity of 20/500 or worse; 12 (92%) of the 13 improved with surgery, and ten (77%) attained best postoperative visual acuity of 20/200 or better.

Visual acuity decreased by more than one Snellen line during the postoperative period in five eyes (23%) as a result of subfoveal neovascularization (Patients 1, 5, and 21) or recurrence of submacular hemorrhage (Patients 3 and 14). Additionally, retinal detachment occurred in three eyes (14%) (Patients 4, 9, and 14) but did not decrease visual acuity and was treated successfully by scleral buckling.

Of the four eyes in which submacular hemorrhage recurred (Patients 1, 3, 6, and 14), two had massive hemorrhage and two had minimal hemorrhage. Patients with massive recurrent subretinal hemorrhage (Patients 3 and 14) had visual acuities in the affected eyes of counting fingers and light perception, respectively. Patients 1 and 6 had minimal recurrent subretinal hemorrhage, and the hemorrhage did not decrease visual acuity. Recurrent subretinal hemorrhage in the two patients with massive hemorrhage was treated by repeat vitrectomy with injection of tissue plasminogen activator and squeezing out with perfluorocarbon liquid. Although visual acuity improved, it did not reach the level attained after the first operation.

Subfoveal neovascularization persisted or developed in seven eyes (Patients 1, 3, 5, 10, 12, 17, and 21) on postoperative fluorescein angiogram. Visual acuity decreased in four (57%) of the seven eyes, and all seven eyes had final visual acuity of 20/200 or worse.

An epiretinal membrane formed in three (14%) of the eyes (Patients 9, 15, and 17), but visual acuity was restored within one line of best postoperative values by surgical removal of the epiretinal membrane in all three eyes.

Final visual acuity was better than preoperative acuity in 18 (82%) of the 22 eyes, was unchanged in three (14%) eyes, and was worse in one (5%) eye. In 15 eyes (68%), visual acuity improved to 20/200 or better postoperatively (Fig. 2). The factors associated with a postoperative visual acuity worse than 20/200 were submacular hemorrhage duration of greater than 30 days ($P = .0048$) and persistent or new postoperative subfoveal neovascularization ($P = .0136$). Age, gender, preoperative visual acuity, area of submacular hemorrhage, and presence of hemorrhagic pigment epithelial detachment were not statistically significantly associated with a postoperative visual acuity worse than 20/200 (Table).

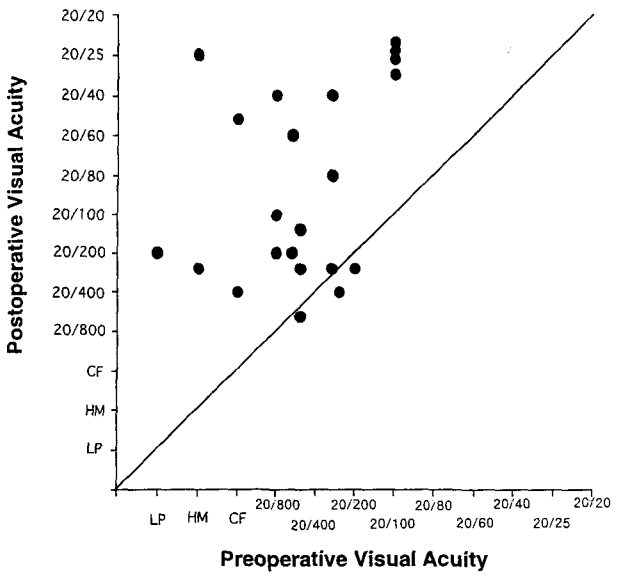

Fig. 2 (Kamei and associates). Scattergram comparing final postoperative visual acuity with preoperative visual acuity in 22 eyes. Dots above the oblique line represent eyes with improved vision after surgery. CF indicates counting fingers; HM, hand motion; and LP, light perception.

DISCUSSION

SURGICAL REMOVAL HAS BEEN PERFORMED FOR SUBMACular hemorrhage associated with age-related macular degeneration in eyes with a poor prognosis for recovery of visual acuity by other methods.[2-5,9,10] However, the results of surgery reported to date have been disappointing: of 87 eyes reported in the literature, only 50 (57%) had improved visual acuity after surgical removal of submacular hemorrhage, and only 18 (21%) of the 87 eyes had postoperative visual acuity of 20/200 or better.

Our results (visual acuity of 20/200 or better in 15 [68%] of 22 eyes) compare favorably with those

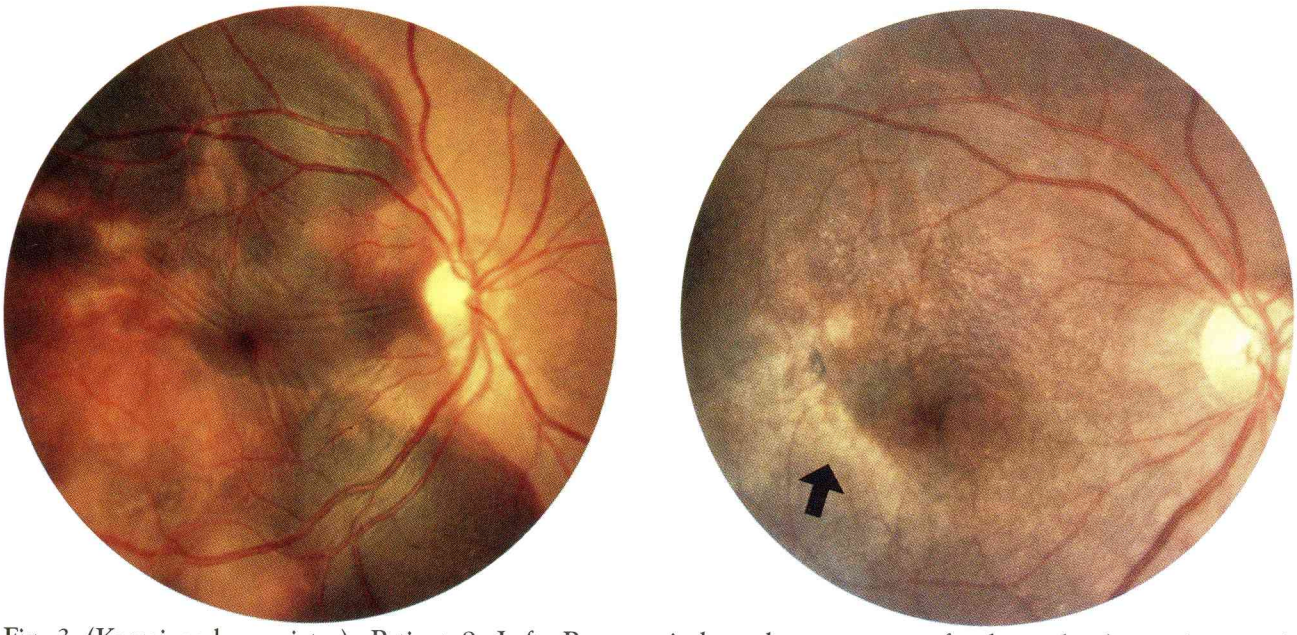

Fig. 3 (Kamei and associates). Patient 9. Left, Preoperatively, a large amount of submacular hemorrhage with hemorrhagic pigment epithelial detachment extends to the temporal half of the fundus. Right, Postoperatively, a retinal pigment epithelial tear was recognized and possibly covered with nonpigmented epithelium (arrow). Visual acuity improved from hand motions to 20/25.

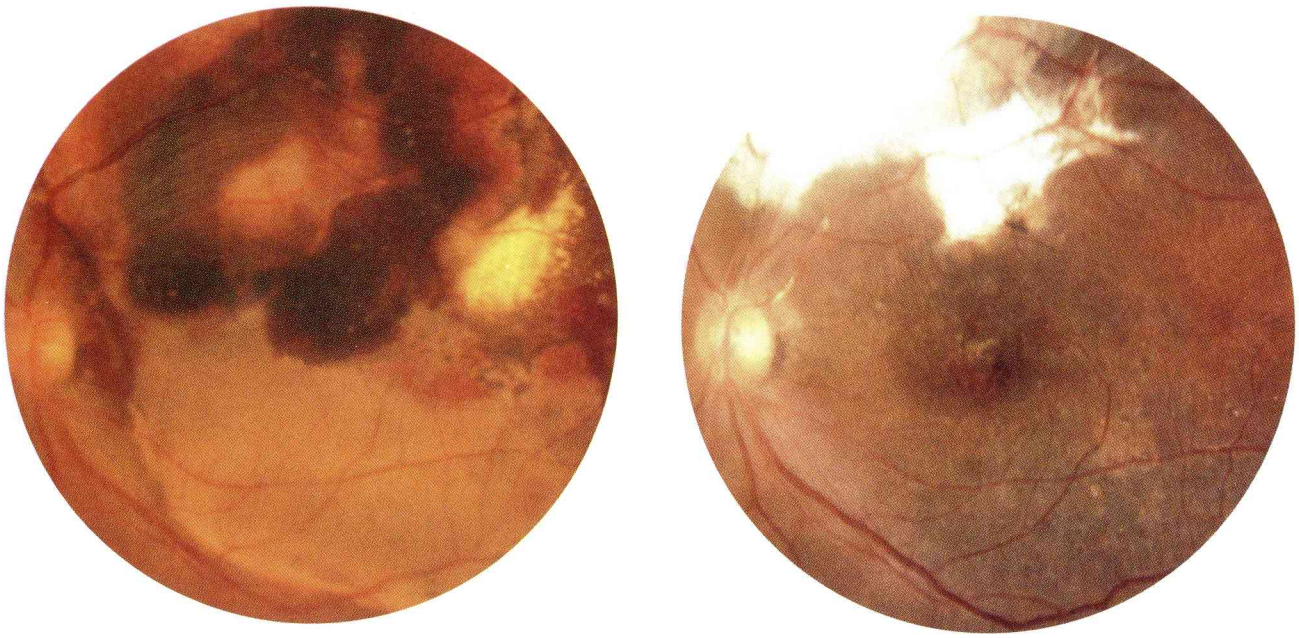

Fig. 4 (Kamei and associates). Patient 4. Preoperative (left) and 18 months postoperative (right) appearance of submacular hemorrhage in a 78-year-old woman. The hemorrhage was unorganized around the macula and organized elsewhere 30 days after bleeding. Visual acuity improved from hand motions to 20/250 after surgery.

previously reported. Of the 22 eyes in our study, 13 (59%) had preoperative visual acuities of 20/400 or worse, and 12 eyes (92%) of the 13 had improved visual acuity postoperatively, with ten (77%) of the 13 attaining best postoperative visual acuity of 20/200 or better. Thus, we believe it is reasonable to presume that a major contributor to our higher success rate is the procedure we used to remove submacular hemorrhage. Injection of tissue plasminogen activator to liquefy the coagulated hemorrhage and application of perfluorocarbon liquid to drain the submacular hemorrhage without manipulation in the subretinal space cause less trauma to the retina than the traditional methods of a large retinotomy, repeated subretinal irrigation or insertion of forceps, or use of a cannulated fluid aspirator to remove subretinal hemorrhage.

Our use of perfluorocarbon liquid to drain submacular hemorrhage into the vitreous cavity has the following advantages over other methods: (1) with liquid perfluorocarbon, hemorrhage under the fovea, which should be given highest priority for removal, is removed first, whereas with other methods hemorrhage is gradually aspirated starting at the retinotomy site; (2) perfluorocarbon liquid promotes evacuation only of liquefied hemorrhage, whereas retinal pigment epithelium may inadvertently be aspirated with active suction in the subretinal space, especially in eyes with age-related macular degeneration, because pigment epithelial detachment may be present as a result of choroidal neovascularization between Bruch's membrane and the retinal pigment epithelium (Fig. 3); and (3) hemorrhage can be evacuated from the vitreous cavity rather than by manipulation of the retina.

Fibrin degradation products, which are derived from the lysis of fibrin, are strongly chemotactic and potent inflammatory agents.[13] Use of tissue plasminogen activator leaves large amounts of fibrin degradation products in the subretinal space. To prevent subsequent chemical damage to photoreceptor cells and retinal pigment epithelial cells, these products must be removed. Thus, we gently flushed the subretinal space with balanced saline solution after fibrinolysis. Although repeated flushing would have cleared more toxic material from the subretinal space, it would also have caused repeated trauma to the retina, so we only used the flush once or twice for each procedure.

To minimize damage to photoreceptor cells, submacular hemorrhage should be removed as soon as possible.[6] Removal of hemorrhage before thrombosis is complete, however, causes the risk of rebleeding. Because no rebleeding occurred when tissue plasminogen activator was used to remove hemorrhage 72 hours after bleeding in an animal model of traumatic hyphema,[14] 72 hours after bleeding may be an optimal time to remove subretinal hemorrhage.

Delay of longer than seven days in removing submacular hemorrhage has been reported as a risk factor for poor outcome of surgery.[9] In the present study, nine (82%) of 11 eyes that had submacular hemorrhage for between eight and 25 days had visual acuity of 20/200 or better after surgery, which was virtually identical to the results of surgery performed seven days or fewer after the onset of hemorrhage. In the latter group, six (86%) of the seven eyes had visual acuity of 20/200 or better. In contrast, none of the four eyes that had submacular hemorrhage for 30 days or longer had visual acuity after surgery of better than 20/200. Surgery was performed in these eyes because they still contained unorganized, red hemorrhagic material at the macula, despite organized white-yellow hemorrhage elsewhere (Fig. 4). The poor results in these eyes, however, suggest that the benefits of surgery are limited when hemorrhage has been present more than 30 days.

Another factor affecting the success of our procedure to remove submacular hemorrhage was the occurrence of subfoveal neovascularization. Subfoveal neovascularization was detected in seven eyes, and none of these eyes maintained a final visual acuity better than 20/200. Thus, finding an effective treatment for persistent subfoveal neovascularization is an area of research that would contribute greatly to restoration of visual acuity.

On the other hand, although no treatment was given for subretinal neovascular membranes, seven eyes (32%) in our study had no subretinal neovascularization on postoperative fluorescein angiography (Fig. 5). Furthermore, a report in the literature documents 18 (75%) of 24 eyes without the occurrence of a choroidal neovascular membrane.[9] There is

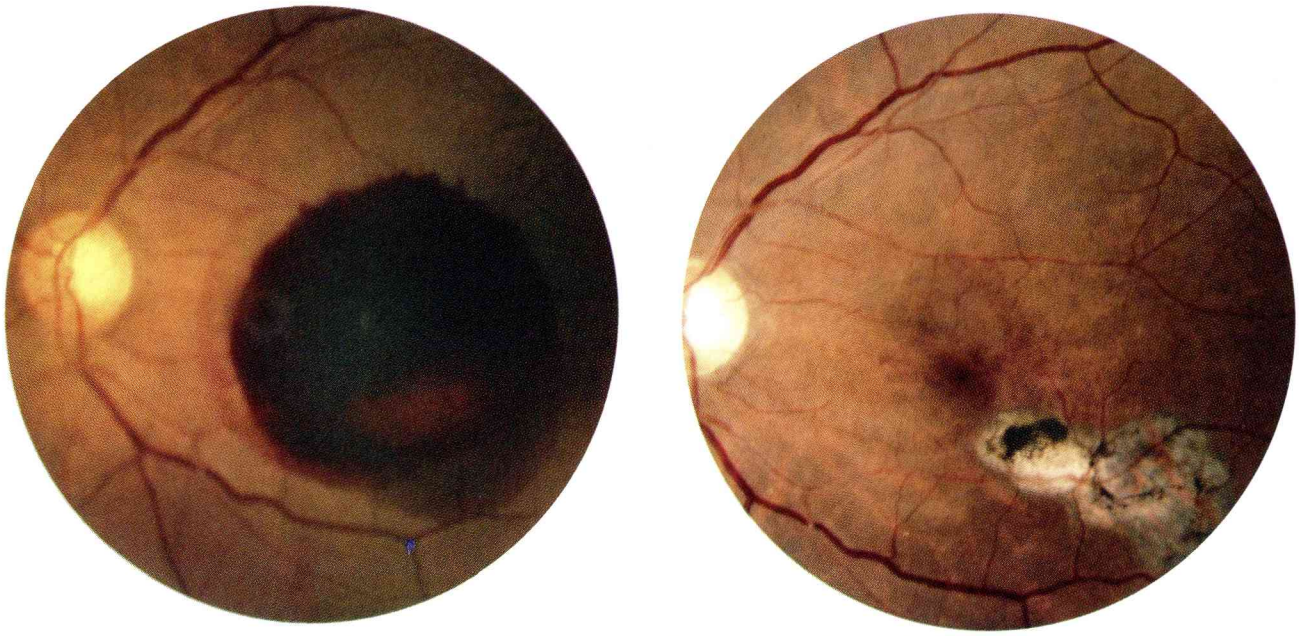

Fig. 5 (Kamei and associates). Patient 11. Left, Preoperatively, preretinal hemorrhage, in addition to thick subretinal hemorrhage centered on the fovea, was seen. Right, One year postoperatively, visual acuity improved from 20/800 to 20/40. No choroidal neovascularization was identified postoperatively.

a speculation in the literature that surgery may promote regression of a choroidal neovascular membrane,[9] but the mechanism of regression of neovascularization is not fully known.

The incidence of epiretinal membrane formation after vitrectomy in our study seemed higher than after vitrectomy for other diseases. This finding may result from the presence of blood, which is a potent stimulator of retinal pigment epithelial or glial proliferation. It has also been speculated that the posterior vitreous attaches to the retina at a higher rate in patients with subretinal neovascularization than in age-matched controls,[12] and residual vitreous cortex after surgical removal may form a nidus for epiretinal membrane formation.

Surgical removal of submacular hemorrhage has the following positive effects: (1) it avoids mechanical damage to the retina caused by fibrin formation and contraction; (2) it reduces retinal toxicity from iron ions; and (3) it restores the metabolic pathway between photoreceptor and retinal pigment epithelial cells. Thus, surgical removal of submacular hemorrhage should lead to improvement in visual acuity if the surgery is performed before retinal damage is irreversible. Our study results show that removal of the hemorrhage using tissue plasminogen activator and perfluorocarbon liquid may improve visual acuity even in patients with risk factors for poor outcome, such as submacular hemorrhage present more than seven days before surgery, presence of hemorrhagic pigment epithelial detachment, or massive subretinal hemorrhage.[9] Minimizing trauma to the retina during surgery plays an important role in the success of the operation and avoidance of postoperative complications. Research directed toward the development of therapies for affected retinal pigment epithelium and photoreceptor cells would also have the potential for improved visual function in patients with age-related macular degeneration.

This study was limited by the lack of a control group, although the natural history of subretinal hemorrhage in age-related macular degeneration is known to be poor.[1] A prospective, randomized, multicenter trial that includes a natural history group would confirm the beneficial results of the current study.

REFERENCES

1. Bennett SR, Folk JC, Blodi CF, Klugman M. Factors prognostic of visual outcome in patients with subretinal hemorrhage. Am J Ophthalmol 1990;109:33–7.
2. Hanscom TA, Diddie KR. Early surgical drainage of subretinal hemorrhage. Arch Ophthalmol 1987;105:1722–3.
3. de Juan E Jr, Machemer R. Vitreous surgery for hemorrhagic and fibrous complications of age-related macular degeneration. Am J Ophthalmol 1988;105:25–9.
4. Wade EC, Flynn HW Jr, Olsen KR, Blumenkranz MS, Nicholson DH. Subretinal hemorrhage management by pars plana vitrectomy and internal drainage. Arch Ophthalmol 1990;108:973–8.
5. Vander JF, Federman JL, Greven C, Slusher MM, Gabel VP. Surgical removal of massive subretinal hemorrhage associated with age-related macular degeneration. Ophthalmology 1991;98:23–7.
6. Toth CA, Morse LS, Hjelmeland LM, Landers MB III. Fibrin directs early retinal damage after experimental subretinal hemorrhage. Arch Ophthalmol 1991;109:723–9.
7. Lewis H, Resnick SC, Flannery JG, Straatsma BR. Tissue plasminogen activator treatment of experimental subretinal hemorrhage. Am J Ophthalmol 1991;111:197–204.
8. Peyman GA, Nelson NC Jr, Alturki W, Blinder KJ, Paris CL, Desai UR, et al. Tissue plasminogen activating factor assisted removal of subretinal hemorrhage. Ophthalmic Surg 1991;22:575–82.
9. Lewis H. Intraoperative fibrinolysis of submacular hemorrhage with tissue plasminogen activator and surgical drainage. Am J Ophthalmol 1994;118:559–68.
10. Ibanez HE, Williams DF, Thomas MA, Ruby AJ, Meredith TA, Boniuk I, et al. Surgical management of submacular hemorrhage. Arch Ophthalmol 1995;113:62–9.
11. Vander JF. Tissue plasminogen activator irrigation to facilitate removal of subretinal hemorrhage during vitrectomy. Ophthalmic Surg 1992;23:361–3.
12. Lambert HM, Capone A Jr, Aaberg TM, Sternberg P Jr, Mandell BA, Lopez PF. Surgical excision of subfoveal neovascular membranes in age-related macular degeneration. Am J Ophthalmol 1992;113:257–62.
13. Sueishi K, Nanno S, Tanaka K. Permeability enhancing and chemotactic activities of lower molecular weight degradation products of human fibrinogen. Thromb Haemost 1981;45:90–4.
14. Williams DF, Han DP, Abrams GW. Rebleeding in experimental traumatic hyphema treated with intraocular tissue plasminogen activator. Arch Ophthalmol 1990;108:264–6.

Reprinted from
American Journal of Ophthalmology
Vol. 121, No. 3, March 1996